

Magnetic knots as the origin of spikes in the gravitational wave backgrounds

Massimo Giovannini*

DAMTP, Silver Street, CB3 9EW Cambridge, United Kingdom

The dynamical symmetries of hot and electrically neutral plasmas in a highly conducting medium suggest that, after the epoch of the electron-positron annihilation, magnetohydrodynamical configurations carrying a net magnetic helicity can be present. The simultaneous conservation of the magnetic flux and helicity implies that the (divergence free) field lines will possess *inhomogeneous* knot structures acting as source “seeds” in the evolution equations of the scalar, vector and tensor fluctuations of the background geometry. We give explicit examples of magnetic knot configurations with finite energy and we compute the induced metric fluctuations. Since magnetic knots are (conformally) coupled to gravity via the vertex dictated by the equivalence principle, they can imprint spikes in the gravitational wave spectrum for frequencies compatible with the typical scale of the knot corresponding, in our examples, to a present frequency range of 10^{-11} – 10^{-12} Hertz. At lower frequencies the spectrum is power-suppressed and well below the COBE limit. For smaller length scales (i.e. for larger frequencies) the spectrum is exponentially suppressed and then irrelevant for the pulsar bounds. Depending upon the number of knots of the configuration, the typical amplitude of the gravitational wave logarithmic energy spectrum (in critical units) can be even four orders of magnitude larger than the usual flat (inflationary) energy spectrum generated thanks to the parametric amplification of the vacuum fluctuations.

Preprint Number: DAMTP-1998-107

to appear in *Physical Review D*

I. INTRODUCTION

The idea that large scale magnetic fields could exist in the early Universe is both appealing and plausible [1]. It was noticed long ago that if magnetic fields existed in the early Universe, they could have affected (or possibly explained) various stages of the formation of cosmic structures [3,4]. Long range stochastic fields can modify the rate of the Universe expansion and the reaction rate at the nucleosynthesis epoch [5]. Stochastic fields coherent over the horizon size at the decoupling time can depolarise the Cosmic Microwave Background Radiation (CMBR) [6], and can also change the sound velocity of the plasma at the corresponding era [7].

If the temperature of the radiation-dominated Universe is higher than the temperature of the electroweak phase transition (i.e. $T > 100$ GeV), then the large scale components of the standard model gauge fields should be identified with the hypermagnetic fields [8] which, by contributing to the (Abelian) anomaly, can generate matter–antimatter fluctuations [9] (possibly relevant in the context of the inhomogeneous nucleosynthesis scenario [10,11]). Long range hypermagnetic fields can also influence the dynamics of the phase transition itself [12]. Interesting consequences of the presence of electroweak condensates for the gravitational wave spectra were also discussed in [13].

Stochastically distributed magnetic fields (either amplified from their vacuum fluctuations [14] through the breaking of the conformal invariance of Maxwell equations or just assumed [15]) can imprint inhomogeneities in the microwave sky. Long ago it was argued that any uniform (spatially homogeneous) magnetic fields can make the energy momentum tensor of a radiation dominated universe slightly anisotropic producing, ultimately, an observable effect in the microwave sky [4]. Recently bounds were derived (using the COBE 4-yrs maps) on the present strength of a uniform (and homogeneous) magnetic field [16].

In this paper we will argue that, on the basis of the physical laws governing the evolution of the mean magnetic fields in a hot plasma, there are no reasons why the topology of the magnetic flux lines should be *trivial*, namely there are no reasons why the magnetic flux lines should not intersect each others. If the topology of the magnetic flux lines is non trivial, then, the helicity of a specific magnetic configuration will also enter in the equations describing evolution of the scalar, vector and tensor fluctuations of the metric in a radiation dominated Universe. Provided the typical scale of the knot (red-shifted at the recombination time) is much smaller than the magnetic Jeans scale at the corresponding epoch, very little impact can be expected for structure formation [17,18].

In short our logic is the following. One of the main features of the evolution equations of the mean magnetic fields (for scales larger than the Debye radius) in highly conducting (and globally neutral) plasmas is that they are

*electronic address: M.Giovannini@damtp.cam.ac.uk

divergence-less (i.e. the field lines have no end points) and, therefore, the structures arising in magnetohydrodynamics (MHD) can be examined in terms of the topology of closed curves [19,20]. Now, it is well known that in (ideal) MHD a unique and intriguing property holds: the *magnetic flux* and *magnetic helicity* are simultaneously conserved all along the evolution of the plasma for scales larger than the magnetic diffusivity scale. Since the Universe is a good conductor all along its history, we have to conclude that, on one hand, thanks to the magnetic flux conservation, the magnetic flux lines always evolve glued together with the plasma element and, on the other hand, thanks to the magnetic helicity conservation, the sum of the number of *twists* and the number of *knots* in the flux lines is also left invariant [19] as time goes by. At this point the choice is twofold. Either we assume (as it is frequently done in the case of stochastic magnetic backgrounds [14,24]) that the (mean) magnetic helicity is strictly zero, or we accept that the magnetic helicity can be present and, in this last case, it will be conserved to a very good approximation.

As we said, a non-vanishing magnetic helicity implies that the corresponding magnetic field configurations must be inhomogeneous (otherwise the integral defining the magnetic helicity cannot be gauge-invariant). Thus, in the present paper, we are forced to deal with inhomogeneous fields. At the same time one could say that inhomogeneous configurations carrying zero (net) magnetic helicity can also have interesting effects on the gravitational wave production. This is certainly true and one of the purposes of the present investigation is to understand, with some specific examples, what difference does it make to drop the (oversimplifying) assumption that the magnetic flux lines of the cosmological magnetic fields have all trivial topological structure.

Inhomogeneous magnetic knots are expected to affect various aspects of the life of our Universe. They can represent a quite interesting source “seed” in the evolution of metric density perturbations during radiation (and possibly matter) dominated epochs. Since magnetic knot configurations with finite energy and helicity are necessarily inhomogeneous, no homogeneous and isotropic (background) contribution is expected from the knot energy-momentum tensor. At the same time, the presence of magnetic knots and twists in the magnetic flux lines does modify the evolution equations of the metric fluctuations. The spatial components of the knot energy-momentum tensor form a three-dimensional rank two (cartesian) tensor which can be decomposed into irreducible scalar (invariant under three dimensional rotations), vector and tensor parts providing source terms for the evolution equations of the corresponding scalar vector and tensor parts of the metric inhomogeneities. The tensor modes of the metric are automatically invariant under infinitesimal coordinate (gauge) transformations [21]. The components of the knot energy-momentum tensor are also invariant under infinitesimal coordinate transformations because of the absence of any (homogeneous and isotropic) magnetic background.

We want to notice immediately that, one of the main ideas of our investigation is the connection among knot seeds and metric fluctuations. Up to now all the investigations on the existence of large scale magnetic fields were mainly devoted to the study of suitable mechanisms able to explain the large scale “magnetic” structure of the Universe, or more specifically, the existence of galactic (and possibly inter-galactic) magnetic fields [24]. In our study we point out that, if the conservation properties arising in MHD are properly taken into account, then, interesting effects can be foreseen also for the metric fluctuations.

In the first place we would like to motivate magnetic knots configurations on the basis of magnetohydrodynamics (MHD). The idea of magnetic knots might seem, at first sight, a crazy one. In order to make this idea quantitatively plausible we will introduce some explicit MHD solutions describing magnetic knots. It is very important that these field configurations are regular over the whole space, they have finite energy and helicity. They represent then a good framework where the effect of magnetic knots on the metric inhomogeneities can be discussed. The fact that our configurations have finite energy (as also required by considerations related to the $U_{em}(1)$ gauge invariance of the magnetic helicity) implies that the amplitude of the magnetic fields tends to zero for scales larger than the scale of the configuration L_s . For the discussion of the magnetic helicity evolution in a radiation dominated stage of expansion an important tool will be the conformal invariance of the (ideal) MHD equations. Moreover, since we want our MHD description to be fully valid we will also consider times larger than the epoch of electron-positron annihilation.

The second purpose of this investigation are the possible phenomenological consequences of the existence of magnetic knots prior to the decoupling time. We will show that spikes in the gravitational waves energy spectrum [22] can be foreseen and we will compare our results with the typical amplitudes of gravitational waves produced in the context of inflationary models. The amplitude of the “magnetic” spikes depends directly upon the helicity of our configuration and turns out to be substantially larger than the signal of a stochastic gravitational wave background with flat (Harrison-Zeldovich) logarithmic energy spectrum which represents a generic prediction of ordinary inflationary models. The “magnetic spikes” in the gravitational wave spectrum are not constrained by pulsars’s pulses since they are expected to occur in a (present) frequency range $\omega_{dec} < \omega < \omega_{e^+e^-}$ (where $\omega_{dec} \sim 10^{-16}$ Hz and $\omega_{e^+e^-} \sim 10^{-10}$ Hz. In principle we could also expect interesting effects from the Lorentz force term associated with the knot configuration and appearing in the Euler (Navier-Stokes) equation for the density field [17,18] which goes, in MHD, as $\vec{J} \times \vec{H} \sim (\vec{\nabla} \times \vec{H}) \times \vec{H}$. The calculation shows that, since the knot scale is just slightly smaller than the magnetic Jeans scale at the decoupling, effects on structure formation are expected to be mild.

The plan of our paper is then the following. In Sec. II we will recall the basic equations and definitions with particular attention to the Alfvén theorem and to the magnetic helicity theorem. In Sec. III we will introduce the class of configurations with finite energy and helicity. In Sec. IV we will introduce the gravitational effects of the knots and in Sec. V we will focus our attention on the problem of magnetic spikes in the gravitational wave spectrum. Section VI contains our concluding remarks. We made the choice of including in the Appendix different technical results which might be of help for the interested reader.

II. DYNAMICAL SYMMETRIES IN HOT PLASMAS

In a conformally flat metric of Friedman-Robertson-Walker (FRW) type the line element is

$$ds^2 = a^2(\eta)[d\eta^2 - d\vec{x}^2], \quad a(\eta) \sim \eta. \quad (2.1)$$

Since we are going to exploit the Weyl invariance of the Maxwell fields in this type of backgrounds we stress, for our future convenience, that (η, \vec{x}) are the conformal coordinates which are related to the flat coordinates (t, \vec{y}) by the relations $d\eta = dt/a(t)$, $d\vec{x} = d\vec{y}/a(t)$. In the following we will denote by a prime the derivation with respect to conformal time and, when needed (for instance in Sec. III), by the over-dot the derivation with respect to the cosmic time t .

Using the magnetohydrodynamical approximation the evolution equations of Maxwell fields at finite conductivity and diffusivity have to be supplemented by the Navier-Stokes equation. By exploiting conformal invariance they can be written as [9,20,23]

$$\left[\left((p + \rho) \vec{v} \right)' + \vec{v} \cdot \vec{\nabla} \left[(p + \rho) \vec{v} \right] + \vec{v} \vec{\nabla} \cdot \left[(p + \rho) \vec{v} \right] \right] = -\vec{\nabla} p + \vec{J} \times \vec{H} + \nu \left[\nabla^2 \vec{v} + \frac{1}{3} \vec{\nabla} (\vec{\nabla} \cdot \vec{v}) \right], \quad (2.2)$$

$$\vec{H}' + \vec{\nabla} \times \vec{E} = 0, \quad \vec{\nabla} \cdot \vec{E} = 0, \quad (2.3)$$

$$\vec{\nabla} \times \vec{H} = \vec{J} + \vec{E}', \quad \vec{\nabla} \cdot \vec{H} = 0, \quad (2.4)$$

$$\vec{J} = \sigma \left(\vec{E} + \vec{v} \times \vec{H} \right), \quad (2.5)$$

where $\vec{v} = \vec{x}'(\eta)$ is the bulk velocity of the plasma, σ is the conductivity and ν is the shear viscosity coefficient; the curved space quantities appearing in Eqs. (2.2)-(2.5) are related to the flat space ones by the metric rescaling

$$\vec{E} = a^2 \vec{\mathcal{E}}, \quad \vec{H} = a^2 \vec{\mathcal{B}}, \quad \sigma = a \sigma_c, \quad \rho = a^4 \rho_c, \quad p = a^4 p_c, \quad \vec{J} = a^3 \vec{j}, \quad \nu = a^3 \nu_c. \quad (2.6)$$

Notice that in Eqs. (2.3) $\vec{\nabla} \cdot \vec{E} = 0$ is not imposed as an additional equation on the fluid and indeed is not a valid equation for compressional waves which emerge from the theory [20,25]. However, if the plasma is globally neutral on scales much larger than the Debye radius (i.e. $L_D(T) \sim \sqrt{T/(n_e e^2)}$ where n_e is the average electron density) the mean electric fields are effectively divergence free. After the epoch of e^+e^- annihilation (i.e. $T < 0.1$ MeV) we have that $n_e \sim 6.43 \times 10^{-9} x_e \Omega_B h_{100}^2 T^3$, and it turns out that $L_D(T) \sim 1.9 \times 10^{-4} (0.1 \text{ MeV}/T) \text{ cm}$ (x_e is the ionization fraction and Ω_B the baryon density in critical units). If we compare the Debye scale with the horizon distance at $T \sim 0.1$ MeV we have that $L_H(t_{e^+e^-}) \sim 10^{12} \text{ cm} \gg L_D(t_{e^+e^-})$. Therefore, for our purposes the plasma description is indeed appropriate.

The set of MHD equations can be studied with different ‘‘closures’’. Some usual closures [20] are the incompressibility (i.e. $\vec{\nabla} \cdot \vec{v} = 0$) and the adiabaticity, but other closures can be invented depending upon the problem at hand (like the isothermal closure or the closure $\vec{J} = \text{constant}$). Since the evolution of the Universe can be described (within the hot Big-Bang model) by an adiabatic expansion, we can certainly require that $\rho = a^4 \rho_c \sim \text{constant}$ and that $p = \rho/3$. Moreover one can also assume that the fluid is incompressible and in this case, not only the magnetic lines will be divergence-less but also the velocity lines will share the same property. We notice, incidentally, that in the incompressible approximation we can also define a hydrodynamical helicity [27] which allows the topological treatment also for the hydrodynamical part of the system. At the end of Sec. IV we will specifically consider a case where the incompressible closure is relaxed.

In referring the reader to Appendix A for further details concerning the MHD evolution we want only to note that at high conductivity the Alfvén theorem holds

$$\frac{d}{d\eta} \int_{\Sigma} \vec{H} \cdot d\vec{\Sigma} = -\frac{1}{\sigma} \int_{\Sigma} \vec{\nabla} \times \vec{\nabla} \times \vec{H} \cdot d\vec{\Sigma}, \quad (2.7)$$

where Σ is an arbitrary closed surface which moves together with the plasma. If we are in the inertial regime (i.e. $L > L_\sigma$ where L_σ is the magnetic diffusivity length), we can say that the expression appearing at the right hand side is subleading and the magnetic flux lines evolve glued to the plasma element. Moreover, the magnetic helicity \mathcal{H}_M is conserved in the inertial range:

$$\mathcal{H}_M = \int_V d^3x \vec{A} \cdot \vec{H}, \quad \frac{d}{d\eta} \mathcal{H}_M = -\frac{1}{\sigma} \int_V d^3x \vec{H} \cdot \vec{\nabla} \times \vec{H}. \quad (2.8)$$

Concerning Eqs. (2.8) two comments are in order. In Eq. (2.8) the vector potential appears and, therefore it might seem that the expression is not gauge invariant. This is not the case. In fact $\vec{A} \cdot \vec{H}$ is not gauge invariant but, nonetheless, \mathcal{H}_M is *gauge-invariant* since we will define the integration volume in such a way that the magnetic field \vec{H} is parallel to the surface which bounds V and which we will call ∂V . Calling \vec{n} is the unit vector normal to ∂V , the integral defining the magnetic helicity is gauge invariant provided $\vec{H} \cdot \vec{n} = 0$ in ∂V . As we will consider finite energy fields in our examples of Section III we will have that $\vec{H} = 0$ in any part of ∂V (which might be a closed surface at infinity). In Eq. (2.8) the term appearing under integration at the right hand side (i.e. $\vec{H} \cdot \vec{\nabla} \times \vec{H}$) is sometimes called also magnetic helicity (or magnetic gyrotropy) and it is a gauge invariant measure of the diffusion rate of \mathcal{H}_M at finite conductivity. The two theorems given in Eqs. (2.7)–(2.8) are reviewed and proven in Appendix A.

Notice that Eqs. (2.7) and (2.8) are truly dynamical symmetries of the plasma, in the sense that they are not inherent to static MHD configurations. Before ending this section we want to mention a further scale which turns out to be important in the discussion of the large scale effects of primordial magnetic fields, namely the magnetic Jeans scale [17,18]. At $t = t_{dec}$ we have from Eq. (A.12) that $L_\sigma(t_{dec}) \simeq 4.7 \times 10^{10}$ cm whereas the magnetic Jeans scale is, at the same epoch,

$$L_{B_J} \simeq \frac{|\vec{B}(t_{dec})| M_P}{\rho_c(t_{dec})}. \quad (2.9)$$

In a matter-dominated Universe the magnetic Jeans scale evolves like the scale factor. In order to make our estimate more constrained we can assume a field sufficiently strong in order to rotate the polarisation plane of the CMBR at the decoupling [6] (i.e. $|\vec{H}(t_{dec})| \geq 10^{-3}$) and we see that

$$L_{B_J}(t_{dec}) \simeq 10^{21} \text{ cm}. \quad (2.10)$$

From this last numerical estimate we see that if the magnetic field is sufficiently strong, the magnetic Jeans length is of the same order of the horizon size (i.e. $L_H(t_{dec}) \sim L_{B_J}(t_{dec})$). This result has interesting implications for the possible impact of magnetic field on structure formation. In particular, we have that if $L_{B_J}(t_{dec}) \sim L_H(t_{dec})$, then the density contrast induced by the Lorentz force term of Eqs. (2.2) and (A.17) can be of order 1 at the time of galaxy formation [17]. In the opposite case (i.e. $L_{B_J}(t_{dec}) \ll L_H(t_{dec})$), from the Lorentz force term we cannot expect any significant effect on structure formation. In Sec. V we will come back to this problem.

III. MAGNETIC KNOT CONFIGURATIONS

Since both magnetic helicity and magnetic flux are conserved during the dynamical evolution in the inertial range, configurations with non trivial topological structure present at some initial time will be preserved all along the dynamical evolution.

In this Section we will provide some examples of magnetic knot configurations. In order to perform various calculations, it is useful to employ configurations which are non singular at large and small distances. In this way all the integrals defining the helicity, the gyrotropy and the total energy. will be automatically well defined. This is exactly what happens in the following examples. Consider the magnetic field with (spherical) components

$$H_r(\mathcal{R}, \theta, n) = -\frac{4B_0}{\pi L_s^2} \frac{n \cos \theta}{[\mathcal{R} + 1]^2}, \quad H_\theta(\mathcal{R}, \theta, n) = -\frac{4B_0}{\pi L_s^2} \frac{\mathcal{R}^2 - 1}{[\mathcal{R}^2 + 1]^3} n \sin \theta, \quad H_\phi(\mathcal{R}, \theta) = -\frac{8B_0}{\pi L_s^2} \frac{r \sin \theta}{[\mathcal{R}^2 + 1]^3} \quad (3.1)$$

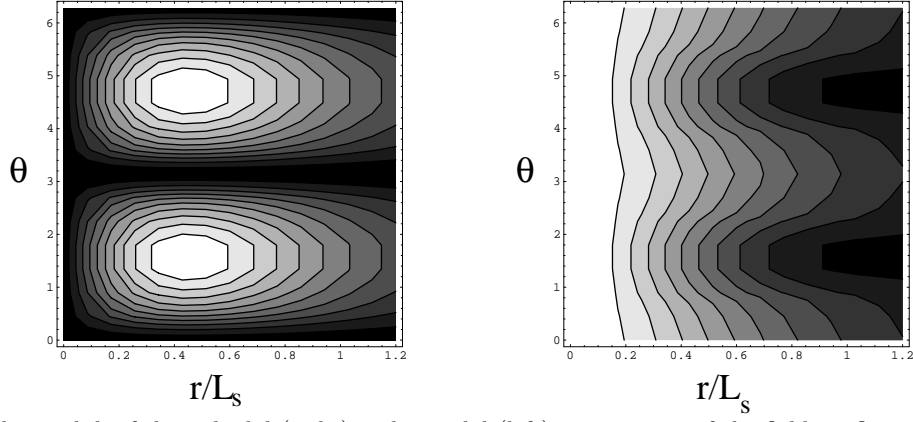


FIG. 1. We plot the moduli of the poloidal (right) and toroidal (left) components of the field configurations reported in Eq. (3.1). In these topographic maps dark regions correspond to low intensity spots of the field whereas brighter regions correspond to higher intensities. The toroidal component does not depend on n . The poloidal component is instead computed in the case of $n = 100$. Moreover in both case we took $|\vec{H}_0(t_{dec})| \sim 0.001$ Gauss. Notice that in the limit of $n \rightarrow 0$ the poloidal component goes to zero. For $r = L/L_s > 2$ the field intensity is suppressed.

In Eq. (3.1) L_s represent the typical scale of the seed and $\mathcal{R} = r/L_s$. Moreover $B_0 = H_0 L_s^2$ is the dimensionless amplitude of the magnetic field; n is just an integer number. It can be also intuitively useful to report explicitly the moduli of the poloidal and toroidal components of \vec{H}

$$|\vec{H}_p(\mathcal{R}, \theta, n)| = \frac{4B_0}{\pi L_s^2} n \frac{\sqrt{\mathcal{R}^4 + 2\mathcal{R}^2 \cos 2\theta + 1}}{[\mathcal{R}^2 + 1]^3}, \quad |\vec{H}_t(\mathcal{R}, \theta)| = \frac{8B_0}{\pi L_s^2} \frac{\mathcal{R} \sin \theta}{[\mathcal{R}^2 + 1]^3} \quad (3.2)$$

where the poloidal and toroidal components of the field are defined in the standard way ($\vec{H}_p = H_r \vec{e}_r + H_\theta \vec{e}_\theta$, $\vec{H}_t = H_\phi \vec{e}_\phi$). The configurations (3.1) were firstly introduced in [28] in the context of the study of the topological properties of the electromagnetic flux lines.

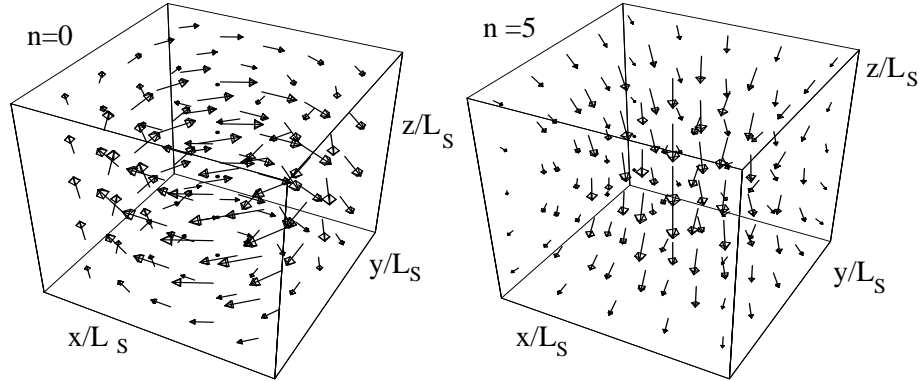


FIG. 2. We plot the magnetic field in Cartesian components (see Eqs. (B.1) in Appendix B) for the cases $n = 0$ (zero helicity) and $n = 5$. The direction of the arrow in each point represents the tangent to the flux lines of the magnetic field, whereas its length is proportional to the field intensity. We notice that for large n the field is concentrated, in practice, in the core of the knot (i.e. $r/L_s < 1$). This can be also argued from Fig. (1).

From the explicit expressions of the vector potentials

$$\begin{aligned} A_r(\mathcal{R}, \theta) &= -\frac{2B_0}{\pi L_s} \frac{\cos \theta}{[\mathcal{R}^2 + 1]^2}, & \mathcal{A}_r(\mathcal{R}, \theta, \eta) &= \frac{A_r(\mathcal{R}, \theta)}{a(\eta)}, \\ A_\theta(\mathcal{R}, \theta) &= \frac{2B_0}{\pi L_s} \frac{\sin \theta}{[\mathcal{R}^2 + 1]^2}, & \mathcal{A}_\theta(\mathcal{R}, \theta, \eta) &= \frac{A_\theta(\mathcal{R}, \theta)}{a(\eta)}, \\ A_\phi(\mathcal{R}, \theta, n) &= -\frac{2B_0}{\pi L_s} \frac{n\mathcal{R} \sin \theta}{[\mathcal{R}^2 + 1]^2}, & \mathcal{A}_\phi(\mathcal{R}, \theta, \eta) &= \frac{A_\phi(\mathcal{R}, \theta)}{a(\eta)}, \end{aligned} \quad (3.3)$$

the magnetic helicity can be computed

$$\mathcal{H}_M = \int_V \vec{A} \cdot \vec{H} d^3x = \int_0^\infty \frac{8nB_0^2}{\pi^2} \frac{\mathcal{R}^2 d\mathcal{R}}{[\mathcal{R}^2 + 1]^4} = nB_0^2. \quad (3.4)$$

Notice that the integration is perfectly convergent over the whole space and, since the field is $\vec{H} = 0$ in any part of ∂V at infinity, this quantity is also gauge invariant. We can compute also the total energy of the field, namely

$$E = \frac{1}{2} \int_V d^3x |\vec{H}|^2 = \frac{B_0^2}{2L_s} (n^2 + 1). \quad (3.5)$$

The magnetic configurations we just presented are solutions of the MHD equations (in the inertial range) with large Prandtl number and small β parameter ($\beta \ll 1$, $Pr_M \gg 1$) for a velocity field $\vec{v} = \pm \vec{H}/[\rho + p]$ (see Appendix A for more detailed explanation of these notations).

In the limit $n \rightarrow 0$ the total helicity goes to zero and, as a consequence, the magnetic field is purely toroidal. In the case where the helicity is non vanishing we can also compute the volume integral of the magnetic gyrotropy $\vec{H} \cdot \vec{\nabla} \times \vec{H}$ which, according to Eq. (2.8), measures the diffusion rate of \mathcal{H}_M at finite conductivity. From Eq. (3.1) we have that

$$\int_V \vec{H} \cdot \vec{\nabla} \times \vec{H} d^3x = \frac{256 B_0^2 n}{\pi L^2} \int_0^\infty \frac{\mathcal{R}^2 d\mathcal{R}}{(1 + \mathcal{R}^2)^5} = \frac{5\mathcal{H}_M}{L_s^2}. \quad (3.6)$$

Using this last result into Eq. (2.8) we obtain the explicit version of the helicity dilution equation valid in the context of our configurations, namely

$$\frac{d}{d\eta} \mathcal{H}_M = -\frac{5}{\sigma L_s^2} \mathcal{H}_M. \quad (3.7)$$

IV. GRAVITATIONAL WAVES AND MAGNETIC KNOTS

Magnetic knot configurations present right after the epoch of electron-positron annihilation can act as seed sources for the evolution equations of the scalar, vector and tensor metric fluctuations. In fact, the spatial part of the knot energy momentum tensor (computed in Eqs. (B.5) of Appendix B) is a symmetric three-dimensional tensor of rank two with six degrees of freedom which transform differently under three-dimensional rotations on the $\eta = \text{constant}$ hypersurface. More precisely the spatial components of the knot energy-momentum tensor can be decomposed in a trace part plus a traceless scalar with one (scalar) degree of freedom each, and vector and tensor parts with two degrees of freedom each. The energy momentum tensor of the knot has no homogeneous background contribution. This fact has two important consequences. On one hand the knot does not affect the background evolution of a radiation (or matter) dominated Universe, on the other hand the energy momentum tensor is automatically invariant for infinitesimal (gauge) coordinate transformations. In the following discussion we will focus our attention on the evolution of the tensor modes. The tensor modes of the metric correspond to gravitational waves [22].

Consider then a perturbation of a (homogeneous and isotropic) conformally flat metric

$$g_{\mu\nu} \rightarrow g_{\mu\nu}(\eta) + \delta g_{\mu\nu}(\vec{x}, \eta). \quad (4.1)$$

whose fluctuating part, $\delta g_{\mu\nu}$, contains scalar, vector and tensor modes

$$\delta g_{\mu\nu}(\vec{x}, \eta) = \delta g_{\mu\nu}^{(S)}(\vec{x}, \eta) + \delta g_{\mu\nu}^{(V)}(\vec{x}, \eta) + \delta g_{\mu\nu}^{(T)}(\vec{x}, \eta), \quad (4.2)$$

The corresponding equations of motion will have, as source term, the scalar vector and tensor modes of the knot energy-momentum tensor

$$\delta T_{\mu\nu}(\vec{x}, \eta) = \delta T_{\mu\nu}^{(S)}(\vec{x}, \eta) + \delta T_{\mu\nu}^{(V)}(\vec{x}, \eta) + \delta T_{\mu\nu}^{(T)}(\vec{x}, \eta). \quad (4.3)$$

Tensor perturbations of the metric are constructed using a symmetric three-tensor which satisfies the constraints

$$h_i^i = \nabla_i h_j^i = 0, \quad (4.4)$$

which implies that h_{ij} does not contain parts transforming as scalars or vectors. Therefore the perturbed tensor components of the metric will be

$$\delta g_{00}^T = 0, \quad \delta_{\mu 0}^{(T)} = 0, \quad \delta g_{ij} = -a^2(\eta)h_{ij}(\vec{x}, \eta), \quad (4.5)$$

and the perturbed line element becomes

$$ds^2 = a^2(\eta) \left[d\eta^2 - (\gamma_{ij} + h_{ij}) dx^i dx^j \right], \quad (4.6)$$

where γ_{ij} denotes the spatial part of the background metric. The evolution equations for the tensor modes of the geometry can then be written as

$$\delta G_{\mu\nu}^{(T)} = 8\pi G \delta T_{\mu\nu}^{(T)}, \quad (4.7)$$

where $\delta G_{\mu\nu}^{(T)}$ are the tensor components of the Einstein tensor $G_{\mu\nu} = R_{\mu\nu} - \frac{1}{2}g_{\mu\nu}R$ perturbed according to Eqs. (4.4)–(4.5). Eq. (4.6) equation becomes, in conformal time,

$$h''_{ij} + 2\mathcal{H}h'_{ij} - \nabla^2 h_{ij} = -16\pi G \tau_{ij}^{(T)}. \quad (4.8)$$

Notice that the energy-momentum tensor can be decomposed, in Fourier space, as

$$\begin{aligned} \tau_{ij}(\vec{x}) &= \frac{1}{(2\pi)^{\frac{3}{2}}} \int e^{i\vec{k}\cdot\vec{x}} \tau_{ij}(\vec{k}) d^3k, \quad \tau(\vec{k}) \equiv \tau_{ii}(\vec{k}), \\ \tau_{ij}(\vec{k}) &= \frac{1}{3} \delta_{ij} \tau(\vec{k}) + \left(\hat{k}_i \hat{k}_j - \frac{1}{3} \delta_{ij} \tau^{(S)}(\vec{k}) \right) + \left(\hat{k}_i \tau_j^{(V)}(\vec{k}) + \hat{k}_j \tau_i^{(V)}(\vec{k}) \right) + \tau_{ij}^{(T)}(\vec{k}), \quad \hat{k}_i = \frac{k_i}{|\vec{k}|}, \end{aligned} \quad (4.9)$$

where

$$\begin{aligned} \tau^{(S)}(\vec{k}) &= \frac{3}{2} \hat{k}_i \hat{k}_j \tau_{ij}(\vec{k}) - \frac{1}{2} \tau(\vec{k}), \\ \tau_i^{(V)}(\vec{k}) &= \tau_{im}(\vec{k}) \hat{k}_m - \hat{k}_i \hat{k}_j \tau_{jm}(\vec{k}) \hat{k}_m, \\ \tau_{ij}^{(T)}(\vec{k}) &= \tau_{ij}(\vec{k}) + \frac{1}{2} \left(\hat{k}_i \hat{k}_j - \delta_{ij} \right) \tau(\vec{k}) + \frac{1}{2} \left(\hat{k}_i \hat{k}_j + \delta_{ij} \right) \hat{k}_m \hat{k}_n \tau_{mn}(\vec{k}) - \hat{k}_i \hat{k}_m \tau_{mj}(\vec{k}) - \hat{k}_m \hat{k}_j \tau_{im}(\vec{k}), \end{aligned} \quad (4.10)$$

In Appendix C the Fourier transforms of each component of the energy momentum tensor is reported. Here we will simply discuss the results of the expansions in the two limits relevant for physical applications. For frequencies much larger than the typical frequency of the knot (i.e. $k > k_s \sim L_s^{-1}$) we have that the Fourier transform of each component of the energy momentum tensor is exponentially suppressed $\exp[-k/k_s]$, whereas for small frequencies (infra-red limit) the various components have different power-law behaviours:

$$\begin{aligned} \tau_{xx}(\vec{k}) \sim \tau_{yy}(\vec{k}) &= \frac{B_0^2}{\pi^2 L_s^4 k_s^3} \sqrt{\frac{\pi}{2}} \frac{n^2}{5} \left[1 + \kappa + \mathcal{O}\left(\left(\frac{k}{k_s}\right)^2\right) \right] e^{-\frac{k}{k_s}}, \\ \tau_{zz}(\vec{k}) &= \frac{B_0^2}{\pi^2 k_s^3 L_s^4} \sqrt{\frac{\pi}{2}} \frac{5 - 3n^2}{20} \left[1 + \kappa + \mathcal{O}\left(\left(\frac{k}{k_s}\right)^2\right) \right] e^{-\frac{k}{k_s}}, \\ \tau_{xz}(\vec{k}) &= \frac{B_0^2}{\pi^2 k_s^3 L_s^4} \left[\mathcal{O}\left(\frac{k}{k_s}\right) \right] e^{-\frac{k}{k_s}}, \quad \tau_{yz}(\vec{k}) = \frac{B_0^2}{\pi^2 k_s^3 L_s^4} \left[\mathcal{O}\left(\frac{k}{k_s}\right) \right] e^{-\frac{k}{k_s}}, \quad \tau_{xy}(\vec{k}) = \frac{B_0^2}{\pi^2 k_s^3 L_s^4} \left[\mathcal{O}\left(\left(\frac{k}{k_s}\right)^2\right) \right] e^{-\frac{k}{k_s}}, \end{aligned} \quad (4.11)$$

(\mathcal{O} denotes the Landau symbol; notice that, within the square brackets we gave the infra-red expansion of the Fourier transform, whereas, outside the brackets we kept the leading [ultra-violet] exponential suppression which always factorizes according to the exact results reported in Appendix C). From Eqs. (4.11) we can see that the off-diagonal terms are always subleading (at large scales) if compared with the diagonal ones.

From Eq. (4.8) it is possible to define the (Fourier space) evolution of the two transverse and traceless degrees (metric) of freedom which reads

$$\begin{aligned} h_{ij}(\vec{x}, \eta) &= \frac{1}{(2\pi)^{\frac{3}{2}}} \int d^3k \left[q_{ij}^{(1)} h_{\oplus}(\vec{k}, \eta) e^{i\vec{k}\cdot\vec{x}} + q_{ij}^{(2)} h_{\otimes}(\vec{k}, \eta) e^{i\vec{k}\cdot\vec{x}} \right], \\ \tau_{ij}^{(T)}(\vec{x}, \eta) &= \frac{1}{(2\pi)^{\frac{3}{2}}} \int d^3k \left[q_{ij}^{(1)} \tau_{\oplus}(\vec{k}, \eta) e^{i\vec{k}\cdot\vec{x}} + q_{ij}^{(2)} \tau_{\otimes}(\vec{k}, \eta) e^{i\vec{k}\cdot\vec{x}} \right], \end{aligned} \quad (4.12)$$

with

$$q_{ij}^{(1)}(\vec{k}) = \frac{1}{2} \left[e_i^{(1)}(\vec{k}) e_j^{(1)}(\vec{k}) - e_i^{(2)}(\vec{k}) e_j^{(2)}(\vec{k}) \right], \quad q_{ij}^{(2)}(\vec{k}) = \frac{1}{2} \left[e_i^{(1)}(\vec{k}) e_j^{(2)}(\vec{k}) + e_i^{(2)}(\vec{k}) e_j^{(1)}(\vec{k}) \right]. \quad (4.13)$$

Notice that $\vec{k}/|\vec{k}|$, $\vec{e}_{(1)}$, $\vec{e}_{(2)}$ are three unit vectors orthogonal to each others:

$$\begin{aligned} \frac{\vec{k}}{|\vec{k}|} &\equiv \left(\hat{k}_x, \hat{k}_y, \hat{k}_z \right) = \left(\sin \theta \cos \phi, \sin \theta \sin \phi, \cos \theta \right), \\ \vec{e}_{(1)} &\equiv \left(\frac{\hat{k}_x}{\sqrt{\hat{k}_x^2 + \hat{k}_y^2}}, -\frac{\hat{k}_y}{\sqrt{\hat{k}_x^2 + \hat{k}_y^2}}, 0 \right) = \left(\sin \phi, -\cos \phi, 0 \right), \\ \vec{e}_{(2)} &\equiv \left(\frac{\hat{k}_x \hat{k}_z}{\sqrt{\hat{k}_x^2 + \hat{k}_y^2}}, \frac{\hat{k}_y \hat{k}_z}{\sqrt{\hat{k}_x^2 + \hat{k}_y^2}}, -1 + \hat{k}_z^2 \right) = \pm \left(\cos \theta \cos \phi, \cos \theta \sin \phi, -\sin \theta \right), \end{aligned} \quad (4.14)$$

(the \pm in the last formula refers to the cases when $\theta > \pi/2$ [+] and $\theta < \pi/2$ [-]). After having extracted the tensor modes from the Fourier space components of the energy-momentum tensor we can find, with some algebra, $\tau_{\oplus}(\vec{k})$ and $\tau_{\otimes}(\vec{k})$:

$$\begin{aligned} \tau_{\oplus}(\vec{k}) &= \sqrt{\frac{\pi}{2}} \frac{B_0^2}{\pi^2 L_s^4 k_s^3} \left(\hat{k}_x^2 + \hat{k}_y^2 \right) \mathcal{Q}(k), \quad \tau_{\otimes}(\vec{k}) = -\sqrt{\frac{\pi}{2}} \frac{B_0^2}{\pi^2 L_s^4 k_s^3} \hat{k}_x \hat{k}_y \hat{k}_z \left(\hat{k}_x^2 + \hat{k}_y^2 + 2\hat{k}_z^2 \right) \mathcal{Q}(k), \\ \mathcal{Q}(k) &= \left(\frac{7n^2 - 5}{40} \right) \left[1 + \frac{k}{k_s} + \mathcal{O} \left(\left(\frac{k}{k_s} \right)^2 \right) \right] e^{-\frac{k}{k_s}}. \end{aligned} \quad (4.15)$$

Then the evolution equations for the two polarizations become

$$\begin{aligned} h_{\oplus}'' + 2\mathcal{H}h_{\oplus}' + k^2 h_{\oplus} &= -16\pi G \tau_{\oplus}, \\ h_{\otimes}'' + 2\mathcal{H}h_{\otimes}' + k^2 h_{\otimes} &= -16\pi G \tau_{\otimes}. \end{aligned} \quad (4.16)$$

We solve the evolution equations for h_{\oplus} and h_{\otimes} by requiring that at η_1

$$h_{\oplus}(\eta_1) = h_{\oplus}'(\eta_1) = 0, \quad h_{\otimes}(\eta_1) = h_{\otimes}'(\eta_1) = 0, \quad (4.17)$$

with the result that

$$\begin{aligned} h_{\oplus}(\vec{k}, \eta) &= \frac{16\pi G}{k^2} \tau_{\oplus}(\vec{k}) \left\{ \frac{k\eta_1 \cos[k(\eta - \eta_1)] + \sin[k(\eta - \eta_1)] - k\eta}{k\eta} \right\}, \\ h_{\otimes}(\vec{k}, \eta) &= \frac{16\pi G}{k^2} \tau_{\otimes}(\vec{k}) \left\{ \frac{k\eta_1 \cos[k(\eta - \eta_1)] + \sin[k(\eta - \eta_1)] - k\eta}{k\eta} \right\}. \end{aligned} \quad (4.18)$$

Using these expression we can compute the energy density of the produced gravitational waves. Up to now we were dealing only with one configuration. In principle after the epoch of electron-positron annihilation different configurations can be present. If the configurations are not correlated the polarisations of the produced gravitational waves will also be stochastically distributed, which means that

$$\langle q_{ij}^{(s)}(\vec{k}) q_{(s')}^{ij}(\vec{k}') \rangle = \delta_{ss'} \delta^{(3)}(\vec{k} - \vec{k}'), \quad (4.19)$$

where $\langle \dots \rangle$ denotes a stochastic average. The total energy density radiated in gravitational waves will then be [29]

$$\rho_{GW}(\eta) = \frac{1}{256\pi^3 a^2} \int d^3k \left\{ |h_{\oplus}'|^2 + |h_{\otimes}'|^2 + k^2 \left[|h_{\oplus}|^2 + |h_{\otimes}|^2 \right] \right\}, \quad (4.20)$$

which implies

$$\rho_{GW}(\eta) = \frac{G}{2\pi} \frac{\eta^2}{a^2} \int \left[\tau_{\oplus}^2 + \tau_{\otimes}^2 \right] \mathcal{F}(k\eta) d^3k, \quad (4.21)$$

where

$$\begin{aligned}
\mathcal{F}(k\eta) = & \left\{ \frac{1}{(k\eta)^6} + \frac{2}{(k\eta)^4} + \frac{2}{(k\eta)^2} + \frac{1}{(k\eta)^4} \left(\frac{\eta_1}{\eta} \right)^2 + \frac{2}{(k\eta)^2} \left(\frac{\eta_1}{\eta} \right)^2 - \frac{4}{(k\eta)^3} \left(\frac{\eta_1}{\eta} \right) \cos [k(\eta - \eta_1)] \right. \\
& + \left[\frac{1}{(k\eta)^4} \left(\frac{\eta_1}{\eta} \right)^2 - \frac{4}{(k\eta)^3} \frac{\eta_1}{\eta} - \frac{1}{(k\eta)^6} \right] \cos [2k(\eta - \eta_1)] - \frac{4}{(k\eta)^3} \sin [k(\eta - \eta_1)] \\
& \left. + \left[\frac{2}{(k\eta)^3} \left(\frac{\eta_1}{\eta} \right)^2 + \frac{2}{(k\eta)^5} \left(\frac{\eta_1}{\eta} \right) - \frac{2}{(k\eta)^5} \right] \sin [2k(\eta - \eta_1)] \right\}. \tag{4.22}
\end{aligned}$$

Define now the comoving frequency $\omega = k/a$ and recall that $k\eta = \omega/H$ (where $H = \dot{a}/a$ is the Hubble factor in cosmic time). By taking η_1 around the epoch of electron positron annihilation (i.e. $T \sim 0.1$ MeV) we can compute $\mathcal{F}(k\eta)$ at any interesting time η_0 as a function of the frequency. Taking $\eta_0 \simeq \eta_{dec}$ (when $T \simeq 0.26$ eV) the (present) decoupling frequency will be $\omega_{dec} \sim 10^{-16}$ Hz whereas the frequency corresponding to the present horizon will be $\omega_0 \sim 3.2 \times 10^{-18} h_{100} \text{Hz}$. The present frequency corresponding to $T \sim 0.1$ MeV is $\omega_s \sim 10^{-11}$ Hz and for the range $\omega_{dec} < \omega < \omega_s$ we have that $|\mathcal{F}(k\eta_{dec})| = |\mathcal{F}(\omega/\omega_{dec})| \sim (\omega/\omega_{dec})^{-2}$.

V. MAGNETIC SPIKES IN THE GRAVITATIONAL WAVE SPECTRUM

For the discussion of the gravitational wave spectra produced by magnetic knots, it is useful to define the energy spectrum in critical units,

$$\Omega_{GW}(\omega, t) = \frac{1}{\rho_{crit}} \frac{d\rho_{GW}}{d \log \omega}, \tag{5.1}$$

which will allow a comparison with the spectra produced, via gravitational instability, in the context of ordinary inflationary model. Using Eqs. (4.15) into Eqs. (4.20) and (4.21) we can perform the angular integration over the momenta and we are left with the integration over $d \log k$. Passing to the physical frequencies and using Eq. (5.1) we get that

$$\Omega_{GW}(\omega, t) \simeq \frac{3}{16\pi^5} \frac{799}{4096} \Omega_\gamma(t) \Lambda^2 \left(\frac{7n^2 - 5}{20} \right)^2 \left(\frac{\omega}{\omega_s} \right) \left(\frac{\omega_{dec}}{\omega_s} \right) \left\{ 1 + O \left(\left(\frac{\omega}{\omega_s} \right)^2 \right) \right\} e^{-\frac{\omega}{\omega_s}}, \quad \omega_{dec} < \omega < \omega_s \tag{5.2}$$

(notice that $\Lambda = H_0^2/\rho = \mathcal{B}_0^2(t)/\rho_c(t)$ and $\Omega_\gamma(t)$ is simply the fraction of critical energy density present in the form of radiation at a given observation time t). For the purposes of the present Section it is also useful to introduce the logarithmic energy spectrum for the knot energy density

$$\Omega_{KN}(\omega, t) = \frac{1}{\rho_{crit}} \frac{d\rho_{KN}}{d \log \omega}, \tag{5.3}$$

where $\rho_{KN}(\vec{k})$ is given by $\tau_{00}(\vec{k})$ after the integration over the directions of \vec{k} . Using Eqs. (C.1) and (C.2) we get that, in the range $\omega_{dec} < \omega < \omega_s$,

$$\Omega_{KN}(\omega, t) \simeq \frac{1}{\pi^3} \Omega_\gamma(t) (n^2 + 1) \Lambda \left(\frac{\omega}{\omega_s} \right)^3 \left[1 + \mathcal{O} \left(\frac{\omega}{\omega_s} \right) \right] e^{-\frac{\omega}{\omega_s}}. \tag{5.4}$$

Obviously, for the consistency of our considerations we have to impose, for all the frequencies and for any time, that $\Omega_{KN}(\omega, t) < 1$. This simply means that the energy density of the knot configurations does not modify the (radiation dominated) background evolution and can be always treated as a small perturbation. Given the analytic form of Eq. (5.4) we see that the largest contribution to $\Omega_{KN}(\omega, t)$ comes from modes of the order of the size of the knot. For higher frequencies the exponential damping becomes effective. Recalling that, today, $\Omega_\gamma(t_0) \simeq 10^{-4}$, the critical energy condition $\Omega_{KN}(\omega, t) < 1$ implies that, for $\omega < \omega_s$,

$$\log_{10} \Lambda + \log_{10}(n^2 + 1) \leq 4.53. \tag{5.5}$$

It is also worth mentioning that in the above region of parameters $\Omega_{GW}(\omega, t) < 1$ is automatically satisfied.

We want now to compare the logarithmic energy spectrum of the gravitational waves produced by magnetic knots with some (possible) inflationary spectra. It is indeed well known that any transition in the curvature inevitably

amplifies the tensor fluctuations of the metric [30–32]. In particular the transition from a primordial inflationary phase to a decelerated one is associated with the production of a stochastic background of gravitational waves [33], which decreases as ω^{-2} for $\omega_0 < \omega < \omega_{dec}$ and stays flat for $\omega_{dec} < \omega < \omega_{dS}$ ($\omega_{dS} = 10^{11} \sqrt{H_{dS}/M_P}$ Hz is the present frequency associated with the maximal curvature scale H_{dS} reached during inflation). The gravitational waves spectrum induced by the inflationary transition can then be written as

$$\begin{aligned}\Omega_{GW}(\omega, t_0) &= \Omega_\gamma(t_0) \left(\frac{H_{dS}}{M_P} \right)^4, & \omega_{dec} < \omega < \omega_{dS}, \\ \Omega_{GW}(\omega, t_0) &= \Omega_\gamma(t_0) \left(\frac{H_{dS}}{M_P} \right)^4 \left(\frac{\omega_{dec}}{\omega} \right)^2, & \omega_0 < \omega < \omega_{dec}.\end{aligned}\quad (5.6)$$

There are various bounds which should be taken into account. At large scale the most significant one comes from the anisotropy of the CMBR [34] which implies that

$$\Omega_{GW}(\omega, t_0) h_{100}^2 < 7 \times 10^{-11}, \quad \text{for } \omega \sim \omega_0. \quad (5.7)$$

For $\omega_{dec} < \omega < \omega_{dS}$, using the bound (5.7) into Eqs. (5.6), we have

$$\Omega_{GW}(\omega, t_0) \leq 10^{-13}, \quad (5.8)$$

or, in terms of H_{dS} [34],

$$\frac{H_{dS}}{M_P} \leq 10^{-6}. \quad (5.9)$$

At intermediate frequencies $\omega \sim 10^{-8}$ Hz, the extreme regularity of the pulsar's pulses [35] imposes

$$\Omega_{GW}(\omega_P, t_0) < 10^{-8}, \quad \text{for } \omega_P \sim 10^{-8}. \quad (5.10)$$

Due to the flatness of the logarithmic energy spectrum of Eq. (5.6) around ω_P , we can clearly see that the pulsar's bound is easily satisfied if Eq. (5.8) is satisfied.

We want now to compare the spectrum given in Eq. (5.2) with the one produced thanks to the inflationary (parametric) amplification of the quantum mechanical fluctuations of the geometry reported in Eq. (5.6). If we look at Eq. (5.2) around ω_s we can see that the gravitational waves produced by the tensor modes of the knot can exceed 10^{-13} (i.e. the maximal allowed amplitude of the inflationary logarithmic energy spectrum in critical units) provided:

$$\log_{10} \Lambda + \frac{1}{2} \log_{10} \left[\left(\frac{7n^2 - 5}{20} \right)^2 \right] > -0.537. \quad (5.11)$$

The last equation was simply obtained by requiring that $\Omega_{GW}(\omega, t)$ given in Eq. (5.2) can be larger than 10^{-13} for $\omega_{dec} < \omega < \omega_s$. In order to be consistent with our approximations we have, therefore to impose simultaneously Eqs. (5.11) and (5.5). The results are reported in Fig. 3 in terms of the two parameter of the model Λ (the intensity of the magnetic field in critical units) and n the number of knots of the configuration.

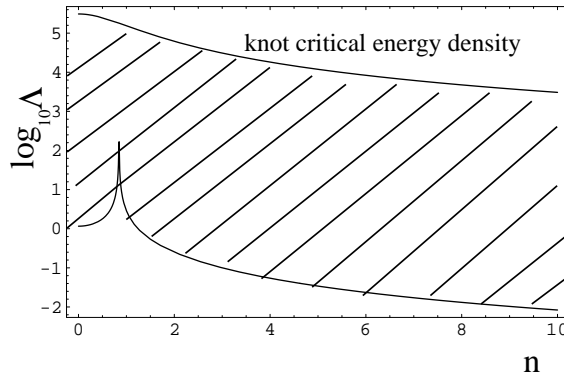


FIG. 3. We report the critical energy density bound applied to the knot configurations (upper line) and the values of the parameters Λ and n necessary in order to give a signal of the same order of the stochastic backgrounds of inflationary origin (lower line). For values of the parameters within the shaded region, the gravitational wave signal produced by the tensor part of the knot energy-momentum tensor exceeds the inflationary prediction also of four orders of magnitude in the (present) frequency range $\omega_s \sim 10^{-11}$ – 10^{-12} Hz. More quantitative illustration is given in Fig. 4.

In Fig. 3 there are, formally, two parameters. One is Λ and the other is n . From the physical point of view, Λ represents the energy scale of the configuration in the limit $n \rightarrow 0$, whereas, n is exactly the magnetic helicity discussed in the previous Sections. We stress the fact that the helicity is conserved for a wide interval of scales after $t_{e^+e^-}$, and, therefore, it represents a very good classical “label” which can be used in order to find the gravitational “imprints” of magnetic knots.

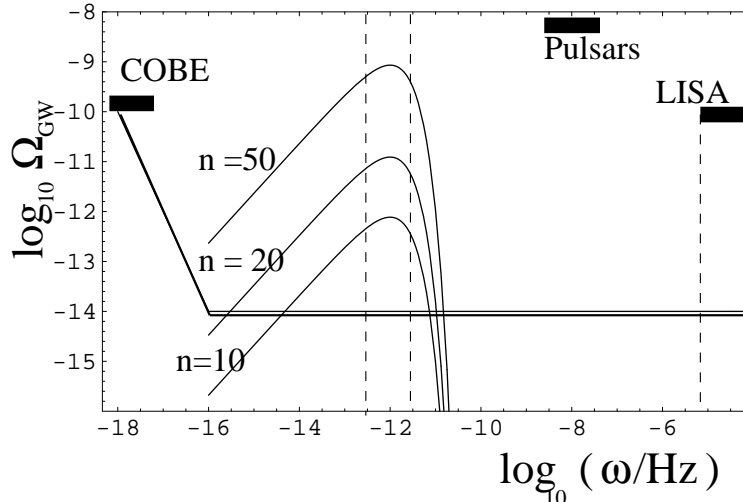


FIG. 4. We report various spikes in the gravitational wave spectrum computed for different values of n . The values of Λ is 3 for the two lower spikes and it is 1 for the upper one. In this plot we reported the expected signal computed assuming that quantum mechanical fluctuations were amplified by the transition between the inflationary phase and radiation dominated phase. Notice that the exponential damping ensures the compatibility with the pulsar bound.

The spectrum of gravitational waves induced by the knot of Eq. (5.2) decreases as (ω/ω_s) for $\omega < \omega_s$ and it is exponentially suppressed for $\omega > \omega_s$. This peculiar behaviour has two important consequences. Firstly, the exponential suppression guarantees that the pulsar bound (see Eq. (5.10)) does not constrain the scenario since at that frequency the gravitational signal of the knot will be suppressed of a factor of the order of $\exp[-\omega_P/\omega_s] \sim \exp(-10^4)$. Secondly, the steep infrared behaviour guarantees a quick suppression at scales even larger corresponding to frequencies of the order of 10^{-16} Hz. Therefore, the signature of these configurations would be compatible with a spike in the gravitational wave spectrum for frequencies of the order of ω_s . Various magnetic spikes are depicted in Fig. 4. We can clearly see that a large magnetic helicity certainly helps in getting a signal which can be substantially larger (four orders of magnitude in Ω_{GW}) than the one provided by the stochastic backgrounds of inflationary origin in the same interval of frequencies. In Fig. 4 we report also the sensitivity of the Laser Interferometer Space Antenna (LISA) for typical (present) frequencies of the order of $\omega_L \simeq 10^{-3} - 10^5$ Hz [36]. We would also like to notice that the spikes we just described are also well below the, so-called, nucleosynthesis bound [37]. In fact the simplest (homogeneous, isotropic) big-bang nucleosynthesis scenario imposes an (indirect) constraint on the gravitational wave spectrum which can be written as [11,22]:

$$\int d \log \omega \Omega_{GW}(\omega, t_0) \leq 0.2 \Omega_\gamma(t_0). \quad (5.12)$$

This constraint implies that $\Omega_{GW}(\omega, t_0)$ should be below 10^{-6} as it occurs for all the modes of our spectrum.

Magnetic knots present right after the epoch of electron-positron annihilation might have, in principle, some influence on the process of galaxy formation. Our discussion will be quite qualitative and will essentially follow the approach of Ref. [17]. Consider the model of a pressure-less fluid made of baryons and of dark matter particles with unperturbed velocity fields $u_B^\mu = (1/a, 0)$, $u_D^\mu = (1/a, 0)$. The velocity fluid perturbations will then be given, generically by $\delta u^i = v^i/a$. Since in our discussion we assumed from the very beginning that $\beta < 1$ (as implied by the critical energy condition on the energy density of the knot) the pressure gradients will also be subleading and, therefore the system for the perturbed density inhomogeneities will be (in the absence of viscous terms)

$$\delta_B'' + \mathcal{H}\delta_B' - \frac{3}{2} \left[\Omega_B \delta_B + \Omega_D \delta_D \right] = \frac{\vec{\nabla} \cdot [\vec{H} \times \vec{\nabla} \times \vec{H}]}{[\rho_D + \rho_B]}, \quad (5.13)$$

$$\delta_D'' + \mathcal{H}\delta_D' - \frac{3}{2} \mathcal{H}^2 \left[\Omega_B \delta_B + \Omega_D \delta_D \right] = 0. \quad (5.14)$$

(5.15)

where $\mathcal{H} = a'/a$ is the Hubble factor in conformal time, $\delta_B = \delta_B/\rho_B$, $\delta_D = \delta\rho_D/\rho_D$ and $\Omega_B = \rho_B/[\rho_B + \rho_D]$, $\Omega_D = \rho_D/[\rho_B + \rho_D]$. In eq. (5.13) the contribution of the Lorentz force has been written by taking into account the fact the electric field are suppressed at high conductivity. Multiplying Eq. (5.13) by Ω_B and Eq. (5.14) by Ω_D we find, after having summed up the two obtained equations, that the total density contrast $\delta = \Omega_B\delta_B + \Omega_D\delta_D$ obeys a decoupled equation

$$\delta'' + \mathcal{H}\delta' - \frac{3}{2}\mathcal{H}^2\delta = \Omega_B \frac{\vec{\nabla} \cdot [\vec{\mathcal{B}} \times \vec{\nabla} \times \vec{\mathcal{B}}]}{[\rho_D + \rho_B]}. \quad (5.16)$$

Notice that, in cosmic time this equation becomes

$$\ddot{\delta} + 2\frac{\dot{a}}{a}\dot{\delta} - \frac{3}{2}\left[\frac{\dot{a}}{a}\right]^2\delta = \Omega_B \frac{\vec{\nabla} \cdot [\vec{\mathcal{B}} \times \vec{\nabla} \times \vec{\mathcal{B}}]}{[a^2(\rho_D + \rho_B)]}. \quad (5.17)$$

The solution of this equation in a matter dominated Universe after recombination ($t > t_{rec}$) can be obtained imposing the initial conditions $\delta(t_{rec}) = 0$ and $\dot{\delta}(t_{rec}) = 0$ with the result that at a given length scale L the density contrast is given by

$$\delta(L, t) = \frac{144}{15\pi^3} \left[\frac{\lambda_{B_J}(t_{rec})}{L_s(t_{rec})} \right]^2 \left[\frac{a(t)}{a(t_{rec})} \right] \mathcal{G}(\lambda, n) \quad (5.18)$$

where $\lambda = L/L_s$ and $\mathcal{G}(\lambda, n)$ contains the spatial dependence. In the case of the configuration given by Eqs. (3.1) $\mathcal{G}(\lambda, n)$ turns out to be:

$$\begin{aligned} \mathcal{G}(\lambda, n) &= P_0(\lambda) + P_n(\lambda), \\ P_0(\lambda) &= \left[4 - 19\lambda^2 + 19\lambda^4 + (27\lambda^2 - 15\lambda^4) \cos 2\theta \right], \\ P_n(\lambda) &= \left[2\lambda^6 - 16\lambda^4 + 19\lambda^2 - 5 - \lambda^2 \left(28 - 13\lambda^2 + \lambda^4 \right) \cos 2\theta \right]. \end{aligned} \quad (5.19)$$

Notice that $\mathcal{G}(\lambda, n)$ receives its maximal contribution around $\lambda = 1$. This simply means that the effect of the Lorentz force term becomes important only for scales comparable with the size of the knot which, in our scenario turns out to be of the order of the horizon size right after the epoch of electron-positron annihilation.

In order to affect structure formation through the Lorentz force we need that, today

$$L_{B_J}(t_0) \sim 0.03 L_s(t_0) \quad (5.20)$$

with $L_s(t_0) \sim 1$ Mpc. From this last condition follows that $\vec{H}(t_{dec}) \sim 10^{-3}$ Gauss. Blue-shifting Eq. (5.20) at the decoupling time we have that

$$L_{B_J}(t_{dec}) \sim 2.7 \times 10^{19} \text{ cm}. \quad (5.21)$$

Now, the typical scale of the knot is $L_s(t_{e^+e^-}) \sim L_H(t_{e^+e^-})$. This means that $L_s(t_{dec}) \sim 10^{18}$ cm. Thus we have that, in our scenario, $L_{B_J} \sim 10 L_s(t_{dec})$. As we just said, in order to have a significant impact on structure formation, we would need $L_s(t_{dec}) \sim L_s(t_{dec})$, whereas, in our case, we have $L_s(t_{dec}) \sim 0.1 L_s(t_{dec})$ which might have some mild impact on structure formation. In the spirit of the order of magnitude estimate presented in the last part of the present Section we notice that, if appreciable effects occur on structure formation (i.e. $|\vec{H}(t_{dec})| \sim 10^{-3}$ Gauss) the very same amplitude of the magnetic field can depolarise the CMBR [6].

VI. CONCLUSIONS

The dynamical symmetries of hot plasmas impose the conservation of the magnetic flux and of the magnetic helicity. In this paper we gave some examples of magnetohydrodynamical configurations carrying a finite magnetic helicity. We argued that, thanks to the helicity conservation the topological properties of the divergence free magnetic field

lines are the only dynamically motivated parameter which could be used in order to discuss the possible implications of magnetic fields in the early Universe.

Based on the fact that after the epoch of electron-positron annihilation the MHD are fully valid we argued that if magnetic knots were present they could have acted as a source for the evolution equation of the scalar, vector and tensor modes of the metric inhomogeneities. We focused our attention on the tensor modes and we found that the induced gravitational wave spectrum is sharply peaked around a (present) frequency of the order of 10^{-11} - 10^{-12} Hz. The typical amplitude of the spike depends upon the helicity of the configuration or, more physically, upon the the number of twists and knots in the magnetic flux lines. The amplitude of the spikes can be substantially larger than the gravitational waves signal provided, in the same interval of frequencies, by inflationary models.

Many interesting points are left for future discussions. First of all there are technical points which could be addressed. In this paper we only took into account the tensor modes. Of course it is certainly possible to extend the above discussion to scalar and vector modes. It is not excluded that some interesting consequences for the small angular scales anisotropies can be addressed. Moreover we would like to stress that the present results hold in the case of one configuration. It would be interesting to generalise these results to more complicated statistical distributions of magnetic knots. This problem has not been addressed in our present investigation.

There are also deeper questions. In this investigation we were dealing with ordinary MHD. It is, in principle possible to extend our discussion to earlier times (like the electroweak epoch) [9,12].

AKNOWLEDGMENTS

I would like to thank M. Shaposhnikov for many useful discussions.

APPENDIX A: MAGNETIC FLUX AND HELICITY THEOREMS

Consider an arbitrary closed surface Σ which moves with the plasma. Then, by definition of the bulk velocity of the plasma (\vec{v} we can also write $d\vec{\Sigma} = \vec{v} \times d\vec{l}$). The (total) time derivative of the flux can therefore be expressed as

$$\frac{d}{d\eta} \int_{\Sigma} \vec{H} \cdot d\vec{\Sigma} = \int_{\Sigma} \frac{\partial \vec{H}}{\partial \eta} \cdot d\vec{\Sigma} + \int_{\partial \Sigma} \vec{H} \times \vec{v} \cdot d\vec{l} \quad (\text{A.1})$$

where $\partial \Sigma$ is the boundary of Σ . Using now the properties of the vector products (i.e. $\vec{H} \times \vec{v} \cdot d\vec{l} = -\vec{v} \times \vec{H} \cdot d\vec{l}$) we can express $\vec{v} \times \vec{H}$ through the Ohm law given in Eq. (2.5) and we obtain that

$$\vec{v} \times \vec{H} = -\vec{E} + \frac{1}{\sigma} \vec{\nabla} \times \vec{H} \quad (\text{A.2})$$

Using now Eq. (A.1) together with the Stokes theorem we obtain

$$\frac{d}{d\eta} \int_{\Sigma} \vec{H} \cdot d\vec{\Sigma} = \int_{\Sigma} \left[\frac{\partial \vec{H}}{\partial \eta} + \vec{\nabla} \times \vec{E} \right] \cdot d\vec{\Sigma} - \frac{1}{\sigma} \int_{\Sigma} \vec{\nabla} \times \vec{\nabla} \times \vec{H} \cdot d\vec{\Sigma} \quad (\text{A.3})$$

From Eq. (2.3) given in Sec. II the first part at the right hand side of Eq. (A.3) is zero and Eq. (2.7), expressing the Alfvén theorem, is recovered.

With a similar technique we can show that the conservation of the magnetic helicity also holds. Consider a closed volume in the plasma, then we can write that $dV = d^3x = \vec{v}_{\perp} \cdot d\vec{\Sigma} d\eta \equiv \vec{n} \cdot \vec{v}_{\perp} d\Sigma d\eta$ where \vec{n} is the unit vector normal to Σ (the boundary of V , i.e. $\Sigma = \partial V$) and \vec{v}_{\perp} is the component of the bulk velocity orthogonal to ∂V . The (total) time derivative of the magnetic helicity can now be written as

$$\frac{d}{d\eta} \mathcal{H}_M = \int_V d^3x \frac{\partial}{\partial \eta} [\vec{A} \cdot \vec{H}] + \int_{\partial V = \Sigma} \vec{A} \cdot \vec{H} \vec{v}_{\perp} \cdot \vec{n} d\Sigma \quad (\text{A.4})$$

By now writing down explicitly the partial derivative at the right hand side of the previous equation we can use the MHD equations (recall that $\vec{E} = -\vec{A}'$ and that $\vec{H} = \vec{\nabla} \times \vec{A}$). Finally using again the Ohm law and transforming the obtained surface integrals into volume integrals (through the divergence theorem) we get to Eq. (2.8).

We want to stress the fact the the magnetic helicity is indeed a gauge invariant quantity under the conditions stated in Sec. II. Consider a gauge transformation

$$\vec{A} \rightarrow \vec{A} + \vec{\nabla} \xi \quad (\text{A.5})$$

then the magnetic helicity changes as

$$\int_V d^3x \vec{A} \cdot \vec{H} \rightarrow \int_V d^3x \vec{A} \cdot \vec{H} + \int_V d^3x \vec{\nabla} \cdot [\xi \vec{H}] \quad (\text{A.6})$$

(in the second term at the right hand side we used the fact that the magnetic field is divergence free). By now using the divergence theorem we can express the volume integral as

$$\int_V d^3x \vec{\nabla} \cdot [\xi \vec{H}] = \int_{\partial V = \Sigma} \xi \vec{H} \cdot \vec{n} d\Sigma \quad (\text{A.7})$$

Now if, as we required, $\vec{H} \cdot \vec{n} = 0$ in ∂V , the integral is exactly zero and \mathcal{H}_M is gauge invariant. Since in Sec. II we considered fields going to zero at infinity $\vec{H} = 0$ in any part of ∂V at infinity. Notice that the field go to zero at infinity is not really necessary. In fact we could just define the integration volume by slicing V in a collection of closed flux tubes. Now by definition of flux tube $\vec{H} \cdot \vec{n} = 0$ if \vec{n} is the unit vector orthogonal to the flux tube.

In order to give a self-contained presentation of our problem we want to recall the main limits where the MHD equations can be discussed. This part of the Appendix represents an ideal follow up of the considerations presented in Section II.

Using the Ohm law of Eq. (2.5) in order to express the induced electric field in terms of the current density and taking into account that $\vec{J} = \vec{\nabla} \times \vec{H}$, we obtain from Eq. (2.4) the standard form of the magnetic diffusivity equation

$$\vec{H}' = \vec{\nabla} \times [\vec{v} \times \vec{H}] + \frac{1}{\sigma} \nabla^2 \vec{H}, \quad \vec{\nabla} \cdot \vec{H} = 0. \quad (\text{A.8})$$

Assuming the incompressible closure together with the adiabatic assumption (i.e. $\rho' = 0$, $p' = 0$) we get a simpler form of the Navier Stokes equation

$$\vec{v}' + [\vec{v} \cdot \vec{\nabla}] \vec{v} = -\frac{1}{p + \rho} \vec{\nabla} \left[p + \frac{|\vec{H}|^2}{2} \right] + [\vec{H} \cdot \vec{\nabla}] \vec{H} + \frac{\nu}{p + \rho} \nabla^2 \vec{v}. \quad (\text{A.9})$$

In writing this equation we used the fact that $2 \vec{J} \times \vec{H} = -\vec{\nabla} |\vec{H}|^2 + 2[\vec{H} \cdot \vec{\nabla}] \vec{H}$. Eqs. (A.8) and (A.9) contain the magnetic and thermal diffusivity scales. We will focus our attention on the case of an electromagnetic plasma whose temperature is $T \ll 100$ GeV (in the opposite limit [$T > 100$ GeV] the equations appearing in the present Section should indeed be generalized to the case of finite chemical potential leading to the anomalous MHD equations [9]). An estimate of the plasma conductivity is necessary for the calculation of the magnetic diffusivity scale. Before the epoch of e^+e^- annihilation (i.e. $T > 2m_e \sim 1$ MeV) the conductivity can be written as $\sigma_c = \lambda T / \alpha_{em}$ where λ is a constant of order unity (recall also that, from Eq. (2.6), $\sigma(\eta) = \sigma_c a(\eta)$). For temperatures smaller than the weak interactions equilibration temperature (i. e. $T < 0.2 m_e$) the electron velocity can be roughly given as $v = \sqrt{T/m_e}$ whereas the collision cross-section is $\sigma_{coll} \simeq (\alpha_{em}/T)^2$ (up to the Coulomb logarithm which is of order one in our case). Therefore the conductivity will be simply estimated by

$$\sigma_c \simeq \frac{\alpha_{em}}{m_e} \frac{1}{\sigma_{coll} v} \simeq \frac{1}{\alpha_{em}} \sqrt{\frac{T^3}{m_e}}. \quad (\text{A.10})$$

From Eq. (A.8) the magnetic diffusivity scale will be

$$L_\sigma(\eta) \sim \sqrt{\frac{\eta}{\sigma_c a(\eta)}} = \sqrt{\frac{t}{\sigma_c}}. \quad (\text{A.11})$$

Using Eq. (A.10) we can say that, after the weak decoupling,

$$L_\sigma(T) \simeq 4.3 \times 10^{10} \left(\frac{T}{0.308 \text{eV}} \right)^{-\frac{7}{4}} \text{ cm}, \quad T < 0.2 m_e \quad (\text{A.12})$$

(where we used as reference the recombination temperature $T_{rec} \sim 0.308$ eV). Notice that this scale is incredibly small if compared with the horizon size at each corresponding epoch. The magnetic diffusivity scale tells us which is the ‘‘inertial’’ [20,26] range of the magnetic field spectrum where the effect of the finite value of the conductivity can be approximately neglected (the so called ideal limit of the MHD equations). The thermal diffusivity coefficient is given by $\nu/(p + \rho) \sim 0.2 \lambda_\gamma(T)$ where

$$\lambda_\gamma(T) \sim 9.106 \times 10^{10} x_e^{-1} (\Omega_B h_{100}^2)^{-1} (\text{MeV}/T)^2 T^{-1} \quad (\text{A.13})$$

(x_e is the ionization fraction and $\Omega_B h_{100}^2$ is the fraction of critical energy density of baryons). Therefore the thermal diffusivity scale will be

$$L_{th}(T) \sim 1.5 \times 10^{16} x_e^{-\frac{1}{2}} (\Omega_B h_{100}^2)^{-\frac{1}{2}} \left(\frac{\text{MeV}}{T} \right)^{\frac{3}{2}} T^{-1}. \quad (\text{A.14})$$

It is important to notice that the ratio of these two quantities gives essentially the (magnetic) Prandtl number [20]

$$Pr_m(T) = 3.5 \times 10^{12} x_e^{-1} (\Omega_B h_{100}^2)^{-1} \left(\frac{\text{MeV}}{T} \right)^{\frac{3}{2}}. \quad (\text{A.15})$$

Since $Pr_m(T_{dec}) \gg 1$ the effect of the Lorentz force terms in Eq. (A.9) cannot be neglected. Another interesting dimensionless ratio is what is usually called β -parameter [20]

$$\beta(T) = \frac{|\vec{H}(T)|^2}{2 p} \sim \frac{45}{2\pi^2 g_{eff}} \frac{|\vec{H}(T)|^2}{T^4} \quad (\text{A.16})$$

If $\beta \ll 1$, then the term $\vec{\nabla}[p + |\vec{H}|^2/2]$ can be neglected. The critical energy condition applied on the magnetic field backgrounds at any given temperature in the radiation dominated epoch enforces by itself this assumption. In order

to give a more quantitative estimate, let us suppose that the magnetic field is strong enough to produce an appreciable depolarisation of the CMBR. If this is the case we should have $|\vec{H}(t_{dec})| \sim 10^{-3}$ Gauss [6] around $T_{dec} \sim 0.26$ eV. This means that $\beta(T_{dec}) \sim 2.7 \cdot 10^{-2}$. Therefore for large Pr_m and small β Eqs. (A.8)–(A.9) can be further simplified:

$$\vec{v}' + [\vec{v} \cdot \vec{\nabla}] \vec{v} = \frac{1}{p + \rho} [\vec{H} \cdot \vec{\nabla}] \vec{H}, \quad (\text{A.17})$$

$$\vec{H}' = \vec{\nabla} \times [\vec{v} \times \vec{H}]. \quad (\text{A.18})$$

APPENDIX B: ENERGY-MOMENTUM TENSOR FOR KNOT CONFIGURATIONS

In this appendix we want to give the components of the energy momentum tensor which are used in our calculations. We want to express the energy-momentum tensor in Cartesian coordinates where some estimates become more tractable. Let us start by giving the cartesian components of the magnetic field:

$$\begin{aligned} H_x(\vec{\mathcal{X}}) &= \frac{4B_0}{\pi L_s^2} \frac{2\mathcal{Y} - 2n\mathcal{X}\mathcal{Z}}{[1 + \mathcal{X}^2 + \mathcal{Y}^2 + \mathcal{Z}^2]^3}, \\ H_y(\vec{\mathcal{X}}) &= -\frac{4B_0}{\pi L_s^2} \frac{2\mathcal{X} + 2n\mathcal{Y}\mathcal{Z}}{[1 + \mathcal{X}^2 + \mathcal{Y}^2 + \mathcal{Z}^2]^3}, \\ H_z(\vec{\mathcal{X}}) &= \frac{4B_0}{\pi L_s^2} \frac{n[\mathcal{X}^2 + \mathcal{Y}^2 - \mathcal{Z}^2 - 1]}{[1 + \mathcal{X}^2 + \mathcal{Y}^2 + \mathcal{Z}^2]^3}, \end{aligned} \quad (\text{B.1})$$

where, as usual, $\mathcal{X} = x/L_s$, $\mathcal{Y} = y/L_s$, $\mathcal{Z} = z/L_s$. The spherical components reported in Eq. (3.1) are simply related to the Cartesian ones. In Cartesian coordinates we have

$$\vec{H}(\vec{\mathcal{X}}) = H_x \vec{e}_x + H_y \vec{e}_y + H_z \vec{e}_z \quad (\text{B.2})$$

where \vec{e}_x , \vec{e}_y and \vec{e}_z are three mutually orthogonal unit vectors. The three unit vectors in spherical polar coordinates are determined by computing the Jacobian matrix with the result that:

$$\begin{aligned} \vec{e}_r &= \frac{\mathcal{X}}{\mathcal{R}} \vec{e}_x + \frac{\mathcal{Y}}{\mathcal{R}} \vec{e}_y + \frac{\mathcal{Z}}{\mathcal{R}} \vec{e}_z, \\ \vec{e}_\theta &= \frac{\mathcal{Z}\mathcal{X}}{\mathcal{R}\sqrt{\mathcal{R}^2 - \mathcal{Z}^2}} \vec{e}_x + \frac{\mathcal{Z}\mathcal{Y}}{\mathcal{R}\sqrt{\mathcal{R}^2 - \mathcal{Z}^2}} \vec{e}_y - \frac{\sqrt{\mathcal{R}^2 - \mathcal{Z}^2}}{\mathcal{R}^2} \vec{e}_z, \\ \vec{e}_\phi &= -\frac{\mathcal{Y}}{\sqrt{\mathcal{X}^2 + \mathcal{Y}^2}} \vec{e}_x + \frac{\mathcal{X}}{\sqrt{\mathcal{X}^2 + \mathcal{Y}^2}} \vec{e}_y. \end{aligned} \quad (\text{B.3})$$

The polar expression for the components of the magnetic fields are obtained, from Eqs. (B.1), (B.2) and (B.3) as $H_r = \vec{H} \cdot \vec{e}_r$, $H_\theta = \vec{H} \cdot \vec{e}_\theta$, $H_\phi = \vec{H} \cdot \vec{e}_\phi$. In order to get to recover the result of Eq. (3.1) the well known relations between spherical and Cartesian coordinates should be used (i.e. $\mathcal{X} = \mathcal{R} \sin \theta \sin \phi$, $\mathcal{Y} = \mathcal{R} \sin \theta \cos \phi$, $\mathcal{Z} = \mathcal{R} \cos \theta$).

Recall now that $\vec{H}(\vec{\mathcal{X}}) = a^2 \vec{\mathcal{B}}$. In terms of $\vec{\mathcal{B}}$ the Maxwell field strength is given by $F_{ij} = a^2 \epsilon_{ijk} \mathcal{B}^k$ and the corresponding energy-momentum tensor will be

$$\delta T_{\mu\nu} = \left(F_{\mu\alpha} F_\nu^\alpha - \frac{1}{4} g_{\mu\nu} F_{\alpha\beta} F^{\alpha\beta} \right) \quad (\text{B.4})$$

(we kept the notation $\delta T_{\mu\nu}$ used in Section 4 in order to stress the fact that $\vec{\mathcal{B}}$ is nothing but a fluctuation on the homogeneous background). It is often useful to express the components of the energy momentum tensor (as we did) in terms of the rescaled fields \vec{H} . The relation between the energy-momentum tensors is $\delta T_{\mu\nu} = a^{-2} \tau_{\mu\nu}$ ($\delta T^{\mu\nu} = a^{-6} \tau^{\mu\nu}$), where now $\tau_{\mu\nu}$ is only expressed in terms of \vec{H} (remember that we work always in conformal time). The components of the Energy-momentum tensor are:

$$\tau_{00}(\vec{\mathcal{X}}) = \frac{8B_0^2}{L_s^4 \pi^2} \frac{4(\mathcal{X}^2 + \mathcal{Y}^2) + n^2 [1 + \mathcal{X}^4 - 2\mathcal{Y}^2 + \mathcal{Y}^4 + 2\mathcal{Z}^2 + 2\mathcal{Y}^2 \mathcal{Z}^2 + \mathcal{Z}^4 + 2\mathcal{X}^2(\mathcal{Y}^2 + \mathcal{Z}^2 - 1)]}{[1 + \mathcal{X}^2 + \mathcal{Y}^2 + \mathcal{Z}^2]^6},$$

$$\begin{aligned}
\tau_{xx}(\vec{\mathcal{X}}) &= \frac{8B_0^2}{L_s^4\pi^2} \frac{4(\mathcal{X}^2 - \mathcal{Y}^2) + 16n\mathcal{X}\mathcal{Y}\mathcal{Z} + n^2[1 + \mathcal{X}^4 - 2\mathcal{Y}^2 + \mathcal{Y}^4 + 2\mathcal{Z}^2 + 2\mathcal{Z}^2\mathcal{Y}^2 + \mathcal{Z}^4 + 2\mathcal{X}^2(\mathcal{Y}^2 - 3\mathcal{Z}^2 - 1)]}{[1 + \mathcal{X}^2 + \mathcal{Y}^2 + \mathcal{Z}^2]^6}, \\
\tau_{yy}(\vec{\mathcal{X}}) &= -\frac{8B_0^2}{L_s^4\pi^2} \frac{4(\mathcal{X}^2 - \mathcal{Y}^2) + 16n\mathcal{X}\mathcal{Y}\mathcal{Z} - n^2[1 + \mathcal{X}^4 - 2\mathcal{Y}^2 + \mathcal{Y}^4 + 2\mathcal{Z}^2 - 6\mathcal{Y}^2\mathcal{Z}^2 + \mathcal{Z}^4 + 2\mathcal{X}^2(\mathcal{Y}^2 + \mathcal{Z}^2 - 1)]}{[1 + \mathcal{X}^2 + \mathcal{Y}^2 + \mathcal{Z}^2]^6}, \\
\tau_{zz}(\vec{\mathcal{X}}) &= -\frac{8B_0^2}{L_s^4\pi^2} \frac{-4(\mathcal{X}^2 + \mathcal{Y}^2) + n^2[1 + \mathcal{X}^4 - 2\mathcal{Y}^2 + \mathcal{Y}^4 + 2\mathcal{Z}^2 - 6\mathcal{Y}^2\mathcal{Z}^2 + \mathcal{Z}^4 + 2\mathcal{X}^2(\mathcal{Y}^2 - 3\mathcal{Z}^2 - 1)]}{[1 + \mathcal{X}^2 + \mathcal{Y}^2 + \mathcal{Z}^2]^6}, \\
\tau_{xy}(\vec{\mathcal{X}}) &= \frac{64B_0^2}{L_s^4\pi^2} \frac{(\mathcal{Y} - n\mathcal{X}\mathcal{Z})(\mathcal{X} + n\mathcal{Y}\mathcal{Z})}{[1 + \mathcal{X}^2 + \mathcal{Y}^2 + \mathcal{Z}^2]^6}, \quad \tau_{xz}(\vec{\mathcal{X}}) = \frac{32B_0^2n}{L_s^4\pi^2} \frac{(-\mathcal{Y} + n\mathcal{X}\mathcal{Z})(\mathcal{X}^2 + \mathcal{Y}^2 - \mathcal{Z}^2 - 1)}{[1 + \mathcal{X}^2 + \mathcal{Y}^2 + \mathcal{Z}^2]^6}, \\
\tau_{yz}(\vec{\mathcal{X}}) &= \frac{32B_0^2n}{L_s^4\pi^2} \frac{(\mathcal{X} + n\mathcal{Y}\mathcal{Z})(\mathcal{X}^2 + \mathcal{Y}^2 - \mathcal{Z}^2 - 1)}{[1 + \mathcal{X}^2 + \mathcal{Y}^2 + \mathcal{Z}^2]^6}. \tag{B.5}
\end{aligned}$$

Concerning this energy-momentum tensor few comments are in order. We did not include any electric field. The reason is simply that all the parts of the energy-momentum tensor containing electric parts are sub-leading at high conductivity. In fact, as we discussed in Section II in our approximations the electric fields are given by $\vec{E} \sim \vec{\nabla} \times \vec{H}/\sigma$ and, therefore, negligible in the ideal approximation of MHD. However, if one would like to study precisely the border region of the ideal approximation (i.e. typical scales of the knot comparable with the magnetic diffusivity scale given by Eq. (A.12)), then, the electric components should be included (sometimes this approximation scheme is named resistive MHD [20]). In our discussion the knot scale L_s is comparable with the magnetic Jeans length and then much larger than the magnetic diffusivity scale. There are interesting limits where the various components of T_μ^ν could be investigated like $n \rightarrow 0$.

APPENDIX C: FOURIER TRANSFORMS OF THE ENERGY-MOMENTUM TENSOR COMPONENTS

In this Appendix we report the Fourier transforms of the components of the energy momentum tensor of our configurations which are crucial for the discussion of the induced inhomogeneities.

$$\begin{aligned}
\tau_{xx}(\vec{k}) &= \frac{8B_0^2}{\pi^2 L_s^4 k_s^3} \left\{ n^2 \left[I_6(\kappa) - \frac{1}{5} I_5(\kappa) \right] + \frac{1}{80} I_4(\kappa) \left[2(n^2 - 2)\kappa_x^2 + 2(n^2 + 2)\kappa_y^2 - 2n^2\kappa_z^2 + 7n^2 \right] \right. \\
&\quad \left. + \frac{n}{240} I_3(\kappa) \left[-n\kappa_x^2 - n(5\kappa_y^2 + \kappa_z^2 + 8i\kappa_x\kappa_y\kappa_z) \right] + \frac{n^2}{1920} I_2(\kappa) \left[\kappa_x^4 + 2\kappa_x^2(\kappa_y^2 - 3\kappa_z^2) + (\kappa_y^2 + \kappa_z^2)^2 \right] \right\}, \\
\tau_{yy}(\vec{k}) &= \frac{8B_0^2}{\pi^2 L_s^4 k_s^3} \left\{ n^2 \left[I_6(\kappa) - \frac{1}{5} I_5(\kappa) \right] + \frac{1}{80} I_4(\kappa) \left[2(n^2 + 2)\kappa_x^2 + 2(n^2 - 2)\kappa_y^2 - 2n^2\kappa_z^2 + 7n^2 \right] \right. \\
&\quad \left. + \frac{n}{240} I_3(\kappa) \left[(2\kappa_y^2 + 2\kappa_z^2 - 5\kappa_x^2) - 8i\kappa_x\kappa_y\kappa_z \right] + \frac{n^2}{5760} I_2(\kappa) \left[\kappa_x^4 + 2\kappa_x^2(\kappa_y^2 + \kappa_z^2) + (\kappa_y^4 - 6\kappa_y^2\kappa_z^2 + \kappa_z^4) \right] \right\}, \\
\tau_{zz}(\vec{k}) &= \frac{8B_0^2}{\pi^2 L_s^4 k_s^3} \left\{ -n^2 I_6(\kappa) + \frac{n^2 + 4}{5} I_5(\kappa) + \frac{1}{80} I_4(\kappa) \left[2n^2\kappa_z^2 - 2(n^2 + 2)\kappa_x - 2(n^2 + 2)\kappa_y \right] \right. \\
&\quad \left. + \frac{n^2}{240} I_2(\kappa) \left[\kappa_x^2 - 2(\kappa_y^2 + 3\kappa_z^2) \right] - \frac{n^2}{1920} I_2(\kappa) \left[\kappa_x^4 + \kappa_z^4 + \kappa_y^2 - 6\kappa_y^2\kappa_z^2 + 2\kappa_x^2(\kappa_y^2 - 3\kappa_z^2) \right] \right\}, \\
\tau_{xy}(\vec{k}) &= \frac{64B_0^2}{\pi^2 L_s^4 k_s^3} \left\{ -\frac{n^2}{1920} I_2(\kappa) \kappa_x \kappa_y \kappa_z^2 - \frac{1}{80} I_4(\kappa) \kappa_x \kappa_y + \frac{n}{480} I_2(\kappa) \left[\kappa_x \kappa_y + i(\kappa_y^2 \kappa_z - \kappa_x^2 \kappa_z) \right] \right\}, \\
\tau_{xz}(\vec{k}) &= \frac{32B_0^2}{\pi^2 L_s^4 k_s^3} n \left\{ \frac{1}{1920} I_2(\kappa) \left[\kappa_x \kappa_z (\kappa_x^2 - \kappa_z^2 + n\kappa_y^2) \right] - \frac{i}{480} I_3(\kappa) \left[\kappa_x^2 \kappa_y + \kappa_y^3 - 8\kappa_z - \kappa_y \kappa_z^2 + \kappa_x (8 - in\kappa_z) \right] \right. \\
&\quad \left. + \frac{1}{160} I_4(\kappa) \left[2n\kappa_x \kappa_z - 3i\kappa_y \right] - \frac{i}{10} I_5(\kappa) \kappa_y \right\}, \\
\tau_{yz}(\vec{k}) &= \frac{32B_0^2}{\pi^2 L_s^4 k_s^3} \left\{ \frac{1}{1920} I_2(\kappa) \left[\kappa_y \kappa_z (\kappa_y^2 - \kappa_z^2 + n\kappa_x^2) \right] + \frac{i}{480} I_3(\kappa) \left[\kappa_x^3 - 8(\kappa_y - \kappa_z) + \kappa_x (48 + \kappa_y^2 - \kappa_z^2 + in\kappa_z) \right] \right. \\
&\quad \left. + \frac{1}{160} I_4(\kappa) \left[3i\kappa_x + 2n\kappa_y \kappa_z \right] \right\},
\end{aligned}$$

$$\begin{aligned}
\tau_{00}(\vec{k}) &= \frac{8B_0^2}{\pi^2 L_s^4 k_s^3} \left\{ \frac{1}{1920} I_2(\kappa) \left[n^2(\kappa_x^4 + \kappa_y^4 + \kappa_z^4) + 2n^2 \kappa_z^2 \kappa_y^2 + 2n^2 \kappa_x^2 \kappa_y^2 + 2\kappa_x^2 \kappa_z^2 \right] + \frac{4-n^2}{5} I_5(\kappa) + n^2 I_6(\kappa) \right. \\
&\quad - \frac{1}{240} I_3(\kappa) \left[3n^2(\kappa_x^4 + \kappa_y^4 + \kappa_z^4) + n^2(\kappa_x^2 + \kappa_y^2 + 2\kappa_z^2) \right] \\
&\quad \left. - \frac{1}{80} I_4(\kappa) \left[15n^2 - 2n^2(\kappa_z^2 + \kappa_x^2 - \kappa_y^2) - 4(\kappa_x^2 + \kappa_y^2) \right] \right\}. \tag{C.1}
\end{aligned}$$

Notice that $\kappa_i \equiv k_i/k_s$ and that $\kappa = \sqrt{\kappa_i \kappa^i}$. In the same way as we reported the Cartesian components of the energy momentum tensor in terms of the ‘‘rescaled’’ coordinates $(\mathcal{X}, \mathcal{Y}, \mathcal{Z}) = (x, y, z)/L_s$, also dealing with the corresponding Fourier components we find useful to work with dimensionless momenta. The fact that we work with κ (instead of with k) also implies that a factor k_s^{-3} appears in front of every component of the Fourier components of the energy-momentum tensor. Concerning Eqs. (C.1) different comments are in order. First of all we can notice that at small scales (i.e. $\kappa > 1$) the Fourier components of the energy momentum tensor are exponentially suppressed as $\exp[-\kappa] = \exp[-k/k_s]$. In other words the typical scale of the knot acts as ultraviolet cut-off. At large scales (i.e. for the infrared branch of the spectrum $k < k_s$) it is of some interest to expand the obtained expressions and we find that

$$\begin{aligned}
\tau_{00}(\vec{k}) &= \frac{B_0^2}{\pi^2 L_s^4 k_s^3} \sqrt{\frac{\pi}{2}} \frac{n^2 + 1}{4} \left[1 + \kappa + \mathcal{O}(\kappa^2) \right], \\
\tau_{xx}(\vec{k}) \sim \tau_{yy}(\vec{k}) &= \frac{B_0^2}{\pi^2 L_s^4 k_s^3} \sqrt{\frac{\pi}{2}} \frac{n^2}{5} \left[1 + \kappa + \mathcal{O}(\kappa^2) \right], \\
\tau_{zz}(\vec{k}) &= \frac{B_0^2}{\pi^2 L_s^4 k_s^3} \sqrt{\frac{\pi}{2}} \frac{5 - 3n^2}{20} \left[1 + \kappa + \mathcal{O}(\kappa^2) \right], \\
\tau_{xz}(\vec{k}) &= \frac{B_0^2}{\pi^2 L_s^4 k_s^3} \mathcal{O}(\kappa), \quad \tau_{yz}(\vec{k}) = \frac{B_0^2}{\pi^2 L_s^4 k_s^3} \mathcal{O}(\kappa), \quad \tau_{xy}(\vec{k}) = \frac{B_0^2}{\pi^2 L_s^4 k_s^3} \mathcal{O}(\kappa^2), \tag{C.2}
\end{aligned}$$

where \mathcal{O} is the Landau symbol. We see that in the infrared limit ($\kappa < 1$) the off-diagonal terms in the energy-momentum tensor are smaller than the diagonal ones. Of course at very small scales (smaller than the size of the knot) the diagonal and off-diagonal terms are damped in the same way. We will use often the following notation

$$\begin{aligned}
\tau_{00}(\vec{k}) &= \frac{B_0^2}{\pi^2 L_s^4 k_s^3} \sqrt{\frac{\pi}{2}} \frac{n^2 + 1}{4} \left[1 + \kappa + \mathcal{O}(\kappa^2) \right] e^{-\kappa}, \\
\tau_{xx}(\vec{k}) \sim \tau_{yy}(\vec{k}) &= \frac{B_0^2}{\pi^2 L_s^4 k_s^3} \sqrt{\frac{\pi}{2}} \frac{n^2}{5} \left[1 + \kappa + \mathcal{O}(\kappa^2) \right] e^{-\kappa}, \\
\tau_{zz}(\vec{k}) &= \frac{B_0^2}{\pi^2 L_s^4 k_s^3} \sqrt{\frac{\pi}{2}} \left(\frac{5 - 3n^2}{20} \right) \left[1 + \kappa + \mathcal{O}(\kappa^2) \right] e^{-\kappa}, \tag{C.3}
\end{aligned}$$

where we kept (in square brackets) the leading infra-red contribution and (outside the brackets) the leading (ultra-violet) damping term. The mathematical reason for this notation is very simple. In doing the ultra-violet expansion of the Fourier transformed components of $\tau_{ij}(\vec{k})$ we can clearly see that the leading exponential damping factorises in the sense that each term appearing in the various components of τ_{ij} is always multiplied by one of the different functions reported in Tab. I. The common feature of all these functions is the exponential damping which becomes effective at small scales and which is connected with the analytical form of the components of \vec{H} which (in real space) all share the $1/(\mathcal{R}^2 + 1)^3$ behaviour. Notice finally that, order by order in κ the trace of $\tau_{\mu\nu}$ vanishes. To lowest order, from Eqs. (C.3) one can immediately check that $\tau_\lambda^\lambda = 0 + \mathcal{O}(\kappa)$.

$I_1(\kappa) = \sqrt{\frac{\pi}{2}} \frac{1}{\kappa} e^{-\kappa}$	$I_2(\kappa) = \frac{1}{2} \sqrt{\frac{\pi}{2}} e^{-\kappa}$
$I_3(\kappa) = \frac{1}{2} \sqrt{\frac{\pi}{2}} (1 + \kappa) e^{-\kappa}$	$I_4(\kappa) = \frac{1}{48} \sqrt{\frac{\pi}{2}} (3 + 3\kappa + \kappa^2) e^{-\kappa}$
$I_5(\kappa) = \frac{1}{384} \sqrt{\frac{\pi}{2}} (15 + 15\kappa + 6\kappa^2 + \kappa^3) e^{-\kappa}$	$I_6(\kappa) = \frac{1}{3840} \sqrt{\frac{\pi}{2}} (105 + 105\kappa + 45\kappa^2 + 103\kappa^3 + \kappa^4) e^{-\kappa}$

TABLE I. We report the coefficients appearing in the Fourier transform of the Cartesian components of the energy-momentum tensor. We recall that, in our notations, $\kappa = |\vec{k}|/k_s$.

-
- [1] Ya. B. Zeldovich, A. A. Ruzmaikin and D. D. Sokoloff, *Magnetic Fields in Astrophysics*, (Gordon and Breach Science Publishers, New York 1983); E. N. Parker, *Cosmical Magnetic Fields*, (Clarendon Press, Oxford, 1979); E. Fermi, Phys. Rev. **75**, 1169 (1949); J. Schwinger, Phys. Rev. **75**, 1912 (1949).
- [2] P. P. Kronberg, Rep. Prog. Phys. **57**, 325 (1994).
- [3] M. J. Rees and M. Rheinhardt, Astr. Astrophys. **19**, 189 (1972).
- [4] Ya. B. Zeldovich and I. D. Novikov, *The Structure and the Evolution of the Universe*, (Chicago University Press, Chicago, 1982).
- [5] G. Greenstein, Nature **223**, 938 (1969); J. J. Matese and R. F. O'Connell, Astrophys. J. **160**, 451 (1970); B. Cheng, A. Olinto, D. N. Schramm and J. Truran, Phys. Rev. D **54**, 4174 (1996); D. Grasso and H. Rubinstein, Astropart. Phys. **3**, 95 (1995) and Phys. Lett. B **379**, 73 (1996); P. Kernan, G. Starkman and T. Vachaspati, Phys. Rev. D **54**, 7207 (1996).
- [6] A. Kosowsky and A. Loeb, Astrophys. J. **461**, 1 (1996); M. Giovannini, Phys. Rev. D **56**, 3198 (1997).
- [7] J. Adams, U. Danielsson, D. Grasso and H. Rubinstein, Phys. Lett. B **388**, 253 (1996).
- [8] M. E. Shaposhnikov, JETP Lett. **44**, 465 (1986); Nucl. Phys. B **287**, 757 (1987); *ibid.* **299**, 797 (1988).
- [9] M. Giovannini and M. Shaposhnikov, Phys. Rev. Lett. **80**, 22 (1998); J. B. Rehm and K. Jedamzik *Big Bang Nucleosynthesis with Matter–Antimatter Domains*, astro-ph/9802255; H. Kurki-Suonio and E. Shvola, in progress.
- [10] K. Kainulainen, H. Kurki-Suonio and E. Shvola, *Inhomogeneous Big-Bang Nucleosynthesis in Light of Recent Observations*, astro-ph/9807098; H. Kurki-Suonio, K. Jedamzik, and G. J. Mathews, Astrophys. J. **43**, 50 (1994); K. Jedamzik and G. M. Fuller, *ibid.* **423**, 33 (1994); K. Jedamzik, G. M. Fuller, and G. J. Mathews, *ibid.* **423**, 50 (1994).
- [11] R. A. Malaney and G. J. Mathews, Phys. Rep. **229**, 145 (1993); S. Sarkar, Rep. Prog. Phys. **59**, 1493 (1996).
- [12] M. Giovannini and M. Shaposhnikov, Phys. Rev. D **57**, 2186 (1998); M. Laine and K. Rummukainen, *The MSSM Electroweak Phase Transition on the Lattice*, hep-lat/9804019; P. Elmfors, K. Enqvist and K. Kainulainen, *Strongly First Order Electroweak Phase Transition Induced by Primordial Hypermagnetic Fields*, hep-ph/9806403.
- [13] D. V. Deryagin, D. Yu. Grigoriev and V. A. Rubakov, Mod. Phys. Lett. A **1**, 593 (1986).
- [14] M. Gasperini, M. Giovannini and G. Veneziano, Phys. Rev. D **52**, 6651 (1995); R. Durrer et al., “*Seeds of Large Scale Anisotropy in String Cosmology*”, CERN-TH-98-069, gr-qc/9804076.
- [15] J. D. Barrow and K. Subramanian, *Microwave Background Signals from tangled Magnetic Fields*, astro-ph/9803261.
- [16] J. Barrow, Phys. Rev. D **55**, 7451 (1997); J. Barrow, P. Ferreira and J. Silk, Phys. Rev. Lett. **78**, 3610 (1997).
- [17] I. Wasserman, Astrophys. J. **224** 337 (1978).
- [18] P. J. E. Peebles, *The Large scale Structure of the Universe*, (Princeton University Press, Princeton, New Jersey 1980).
- [19] M. A. Berger and G. B. Field, J. Fluid Mech. **147**, 133 (1984).
- [20] D. Biskamp, *Non-linear Magnetohydrodynamics* (Cambridge University Press, Cambridge, 1994); N. A. Krall and A. W. Trivelpiece, *Principles of Plasma Physics*, (San Francisco Press, San Francisco 1986).
- [21] J. Bardeen, Phys. Rev. D **22**, 1882 (1980).
- [22] K. S. Thorne, in *300 Years of Gravitation*, edited by S. W. Hawking and W. Israel (Cambridge University Press, Cambridge, England, 1987);
L. P. Grishchuk, Usp. Fiz. Nauk. **156**, 297 (1988) [Sov. Phys. Usp. **31**, 940 (1988)];
B. Allen, in Proceedings of the Les Houches School on Astrophysical Sources of Gravitational Waves, edited by J. Marck and J.P. Lasota (Cambridge University Press, Cambridge England, 1996).
- [23] K. S. Thorne and D. MacDonald, Mon. Not. R. astr. Soc. **198**, 339 (1981); K. A. Holcomb, Astrophys. J. **362**, 381 (1990); C. P. Dettmann, N. E. Frankel and V. Kowalenko, Phys. Rev. D **48**, 5655 (1993); R. M. Gailis, C. P. Dettmann, N. E. Frankel and V. Kowalenko, *ibid.* **50**, 3847 (1993); A. Sil, N. Banerjee and S. Chatterjee, *ibid.* **53**, 7369 (1995); D.T. Son, *Magnetohydrodynamics of the Early Universe and the Evolution of Primordial Magnetic Fields*, hep-ph/9803412.
- [24] M. S. Turner and L. M. Widrow, Phys. Rev. D **37**, 2743 (1988); B. Ratra, Astrophys. J. Lett. **391**, L1 (1992); M. Gasperini, M. Giovannini and G. Veneziano, Phys. Rev. Lett. **75** (1995) 3796; G. Sigl, A. V. Olinto and K. Jedamzik, Phys. Rev. D **55**, 4852 (1997); T. Vachaspati, Phys. Lett. B **265**, 258 (1991); K. Enqvist and P. Olesen, *ibid.*, **319**, 178 (1993); *ibid.* **329**, 195 (1994); T. W. Kibble and A. Vilenkin, Phys. Rev. D **52**, 679 (1995); G. Baym, D. Bodeker and L. McLerran, *ibid.* **53**, 662 (1996); M. Joyce and M. Shaposhnikov, Phys. Rev. Lett. **79** 1193 (1997); K. Enqvist, Int. J. Mod. Phys. D **7**, 331 (1998).
- [25] K. Jedamzik, V. Katalinic, A. V. Olinto Phys. Rev. D **57**, 3264 (1998).
- [26] P. Olesen Phys. Lett. B **398**, 321 (1997).
- [27] K. H. Moffat, J. Fluid. Mech. **35**, 117 (1969); K. Moffat *Magnetic Field Generation in Electrically Conducting Fluids*, (Cambridge University Press, Cambridge 1978).
- [28] A. F. Rañada, J. Phys. A **25**, 1621 (1992); *ibid.* **23** L815 (1990).
- [29] V. F. Mukhanov, H. A. Feldman and R. H. Brandenberger, Phys. Rep. **215**, 203 (1992).
- [30] L. P. Grishchuk, Zh. Eksp. Teor. Fiz. **67**, 825 (1974) [Sov. Phys. JETP **40**, 409 (1975)].

- [31] A. A. Starobinsky, Pis'ma Zh. Eksp. Teor. Fiz. **30**, 719 (1979) [JETP Lett. **30**, 682 (1979)].
- [32] L. P. Grishchuk and M. Solokhin, Phys. Rev. D **43**, 2566 (1991).
- [33] B. Allen, Phys. Rev. D **37**, 2078 (1988); V. Sahni, Phys. Rev. D **42**, 453 (1990); M. Gasperini and M. Giovannini, Phys. Lett. B **282**, 36 (1992); Phys. Rev. D **47**, 1519 (1993); L. P. Grishchuk, Phys. Rev. Lett. **70**, 2371 (1993); M. Giovannini, Phys. Rev. D **55**, 595 (1997); hep-ph/9806329, Phys. Rev. D (in press).
- [34] V. A. Rubakov, M. V. Sazhin and A. V. Veryaskin, Phys. Lett. B **115**, 89 (1982); L. F. Abbott and M. B. Wise, Nucl. Phys. B **244**, 541 (1984); L. P. Grishchuk, Phys. Rev. D **48**, 3513 (1993).
- [35] V. Kaspi, J. Taylor, M. Ryba, Astrophys. J. **428**, 713 (1994).
- [36] K. Danzmann et al., *LISA Pre-Phase A Report*, Report MPQ 208 Max-Planck-Institut, Garching, Germany.
- [37] V. F. Schwartzman, Pis'ma Zh. Eksp. Teor. Fiz. **9**, 315 (1969) [JETP Lett. **9**, 184 (1969)].